Vortex dynamics in type-II superconductors under strong pinning conditions

A. U. Thomann, V. B. Geshkenbein, and G. Blatter
Institute for Theoretical Physics, ETH Zurich, 8093 Zürich, Switzerland
(Received 24 July 2017; revised manuscript received 8 October 2017; published 30 October 2017)

We study effects of pinning on the dynamics of a vortex lattice in a type-II superconductor in the strong-pinning situation and determine the force-velocity (or current-voltage) characteristic combining analytical and numerical methods. Our analysis deals with a small density n_p of defects that act with a large force f_p on the vortices, thereby inducing bistable configurations that are a characteristic feature of strong pinning theory. We determine the velocity-dependent average pinning-force density $\langle F_p(v)\rangle$ and find that it changes on the velocity scale $v_p \sim f_p/\eta a_0^3$, where η is the viscosity of vortex motion and a_0 the distance between vortices. In the small pin-density limit, this velocity is much larger than the typical flow velocity $v_c \sim F_c/\eta$ of the free vortex system at drives near the critical force density $F_c = \langle F_p(v=0)\rangle \propto n_p f_p$. As a result, we find a generic excess-force characteristic, a nearly linear force-velocity characteristic shifted by the critical force density F_c; the linear flux-flow regime is approached only at large drives. Our analysis provides a derivation of Coulomb's law of dry friction for the case of strong vortex pinning.

DOI: 10.1103/PhysRevB.96.144516

I. INTRODUCTION

Superconductors carry electric currents without dissipation [1] and expel magnetic fields from their body, known as the Meissner-Ochsenfeld effect [2]. In a type-II superconductor, magnetic fields H in the range between the lower (H_{c1}) and upper (H_{c2}) critical fields penetrate the material in the form of quantized flux lines ($\Phi_0 = hc/2e$) or vortices, resulting in the mixed or Shubnikov [3] phase. The repulsive interaction mediated by the vortex currents leads to the formation of an Abrikosov vortex lattice [4] with an average induction B inside the sample. A current density j drives the vortices with the Lorentz force density $F_L = jB/c$, giving rise to vortex motion and dissipation. The vortex velocity v is determined by the force balance equation $\eta v = F_L$ with the Bardeen-Stephen viscous coefficient [5] $\eta \sim BH_{c2}/\rho_n c^2$ and ρ_n the normal state resistivity. The resulting electric field $E = Bv/c$ deprives the superconductor from its defining property, to carry electric current without dissipation, with the emerging linear response characterized by the flux-flow resistivity $\rho_{ff} \sim \rho_n B/H_{c2} < \rho_n$.

Material defects lead to vortex pinning [6–8]; they transform the Abrikosov lattice into a disordered phase [9–11] and reestablish the superconductor's ability to carry current free of dissipation. The dissipative force balance equation is augmented by the velocity-dependent mean pinning-force density $\langle F_p(v)\rangle$, $\eta v = F_L - \langle F_p(v)\rangle$, entailing important modifications of the vortex dynamics $v(F_L)$: below the critical force $F_c = \langle F_p(v=0)\rangle$, vortex motion is inhibited; this defines the critical current density $j_c = cF_c/B$. Above depinning at F_c (or for currents $j > j_c$), vortices start moving across defects with an average bulk velocity determined by the velocity dependent pinning-force density $\langle F_p(v)\rangle$. The linear flux-flow behavior with its reduced resistivity ρ_{ff} is assumed only at high drives or velocities. The full force-velocity (F_L-v) characteristic of the superconductor, see Fig. 1, then characterizes the zero temperature vortex dynamics in a complete way. With the driving force F_L proportional to the applied current I and the voltage drop V across the sample proportional to the vortex velocity v, the force-velocity curve is equivalent to the measured current-voltage (or I-V) characteristic. In this paper, we determine the force-velocity (or current-voltage) characteristic (see Fig. 1) of a strongly pinned vortex solid in a generic isotropic type-II superconductor and in the absence of thermal fluctuations.

Vortex pinning has originally been studied for strong pinning centers by Labusch [6] (see also Ref. [7]). Strong pins induce bistable states in the flux-line lattice. They act individually [6] and the direct summation of pinning forces is nonzero, i.e., $j_c \propto n_p$ with n_p the density of defects or pins; collective effects due to other pins result in small corrections. If individual pins are weak, pinning is collective and vortices are only pinned by the joint action of many pinning centers [8]; the direct summation of the forces induced by individual pins averages out to zero and $j_c \propto n_p^2$ for the simplest case of nondispersive weak bulk pinning. The crossover between the regimes of weak collective and strong pinning is given by the Labusch criterion [6], which involves the ratio κ between the steepest force gradient $\partial_x f_p(x)$ (the largest negative curvature) of the pinning potential and an effective elasticity $\bar{C}$ of the lattice. Pinning is strong if the pinning-force gradient dominates the elasticity with $\kappa > 1$. On the other hand, in a very stiff lattice with large elastic constants, we have $\kappa < 1$ and pinning is weak and necessarily collective.

While weak collective pinning has been intensely studied during recent times [10,11], the further development of strong pinning theory has been less dynamic, although some progress has been made [12–16]. The relation between weak collective versus individual strong pinning has been analyzed within a pinning diagram [17] delineating the origin of static critical forces F_c as a function of defect density n_p and strength f_p. Recently, the ac linear response of a field-penetrated superconductor hosting a pinned vortex lattice has been analyzed within the framework of strong pinning theory [18,19]. In the present paper, we focus on the dynamic aspects of strong pinning.

The force-velocity characteristic derives from the dynamical equation for vortex motion:

$$\eta v = F_L(j) - \langle F_p(v)\rangle. \tag{1}$$

The main difficulty with Eq. (1) is in the determination of the velocity-dependent average pinning-force density $\langle F_p(v)\rangle$ (we

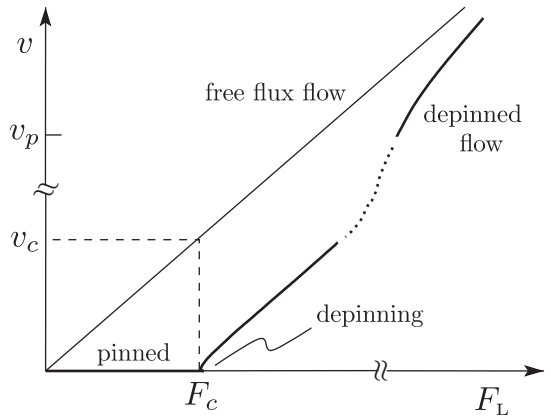

FIG. 1. Sketch of the force-velocity (equivalent to the current-voltage) characteristic of a generic type-II superconductor in the absence of thermal fluctuations. For an external force density F_L smaller than the critical force density F_c, the vortex system remains pinned and $v = 0$. For $F_L > F_c$, vortices are depinned and move with finite velocity $v > 0$; at large drives $F_L \gg F_c$, the characteristic approaches the free flux-flow regime. For strong pinning in the dilute-pin limit, we find an excess-force characteristic, with a linear flux-flow branch shifted by F_c extending over a large regime of velocities v beyond $v_c = F_c/\eta$. The pinning-force density $\langle F_p(v)\rangle$ changes on the velocity scale $v_p \gg v_c$ and the force-velocity characteristic approaches the free flux-flow regime only for $v \gg v_p$.

choose $\langle F_p(v)\rangle$ to be positive). Within the framework of weak collective pinning theory, dimensional [8,10] or perturbative [20,21] estimates have been made and provide results on a qualitative level with a focus on either the perturbative regime at high velocities [20,21] or on the universal regime near depinning [22]. In concentrating on the strong pinning situation, we study the limit of dilute pins, i.e., a small pin-density n_p, and consider defects, which pin at most one vortex line—we call this the single-pin/single-vortex strong pinning regime.

The task of finding the force-velocity characteristic involves three steps: first, we solve the dynamical equation of motion for a vortex line moving along x and crossing the center of a pinning defect. The solution of this "microscopic" problem provides us with the time-dependent displacement field $u(t)$ of the moving vortex and the "elementary" pinning force $f_p[u(t)]$ acting on the vortex line. Second, a proper average over the instantaneous force $f_p[u(t)]$ provides the average pinning force $-\langle f_p(v)\rangle$ per pin acting on the vortex system (with the sign guaranteeing a positive average pinning-force density $\langle F_p(v)\rangle$). This force changes on the microscopic velocity scale $v_p \sim f_p/\eta a_0^3$, which depends on the strength f_p of the individual pins and on the dynamical properties of the vortex system but not on the pin density n_p; here, $a_0^2 = \Phi_0/B$ denotes the inverse vortex density. The force $\langle f_p(v)\rangle$ involves an average along the drive direction x; a second average over the transverse dimension y is required in order to find the average pinning-force density $\langle F_p(v)\rangle$. This average can be cast into the form of a transverse pinning or trapping length $t_\perp(v)$ within which vortices passing the defect are pinned. Since the pins act individually in the small pin-density limit, we obtain the average pinning-force density in the form $\langle F_p(v)\rangle = n_p(2t_\perp/a_0)\langle f_p(v)\rangle$. At $v = 0$, the value of $\langle F_p(v)\rangle$ defines the critical force density F_c. Third, given the driving force density (or current density) F_L, we have to solve the dynamical equation (1) for the velocity v. This macroscopic problem defines a second velocity $v_c = F_c/\eta \propto n_p$, the flow velocity of vortices at F_c in the absence of pinning, and hence the sought force-velocity characteristic involves both a microscopic (v_p) and a macroscopic (v_c) velocity scale.

Since the above scheme essentially describes a one-particle (in fact, one vortex-line) problem, it can be solved via analytical and numerical methods and the results obtained are precise, in opposition to the usual estimates made in weak collective pinning theory. Furthermore, the result in the dilute pin limit (i.e., small n_p) is simple and generic: rewriting the dynamical equation (1) in the form

$$\frac{F_L}{F_c} = \frac{v}{v_c} + \frac{\langle f_p(v/v_p)\rangle}{f_c} \tag{2}$$

makes the dependence on the two velocity scales v_c and v_p explicit. Since $v_c \propto n_p$ involves the pin density n_p, we have $v_c \ll v_p$ and the velocity scales separate in the dilute pin limit. With $\langle f_p(v/v_p)\rangle \approx f_c$ for velocities $v/v_p \ll 1$, we find a characteristic that takes the generic form of an F_c-shifted linear curve,

$$v \approx \frac{1}{\eta}(F_L - F_c), \tag{3}$$

see Fig. 1; the free dissipative flow $v = F_L/\eta$ is approached only at very high velocities $v \gg v_p \gg v_c$. Experiments measuring the current-voltage, i.e., I-V, characteristic then should observe an excess-current characteristic $V = R_{ff}(I - I_c)$ with R_{ff} the flux-flow resistivity; this type of characteristic has been widely measured in the past [23–27] and its microscopic derivation is the main purpose and result of this paper. In doing so, we prove the analog of Coulomb's law of dry friction (describing the motion of a solid body sliding on a dry surface) for the case of strong vortex pinning in the dilute limit; in Amontons' first and second laws of friction, the friction force, corresponding to our F_c, is given by the product of the friction coefficient k and the normal force F_n, $F_f = kF_n$. Amontons' third law or Coulomb's law of dry friction tells, that the kinetic friction at finite velocity is independent of the sliding velocity v, $F_f(v) = F_f = kF_n$. These laws immediately imply a linear excess-force characteristic $v = (F - F_f)\Theta(F - F_f)/\eta$ for the driven (by the force F) body with viscous (η) dynamics and subject to a friction force F_f.

Besides this simple and generic result for the overall shape of the force-velocity characteristic, it is interesting to understand the change in the pinning-force density $\langle F_p(v)\rangle$ with velocity v and the underlying mechanism for this velocity dependence, i.e., the analog of the corrections to Coulomb's law of dry friction. Figure 6 shows the result for the average force $\langle f_p(v)\rangle$ (carrying the main velocity-dependence of $\langle F_p(v)\rangle$) generated by a Lorentzian-shaped pinning potential. For *very strong pinning* with $\kappa \gg 1$, we find a smooth decrease of $\langle f_p(v)\rangle$ with increasing velocity v with three characteristic velocity regions; starting with large velocities $v > \kappa v_p$ and using perturbation theory around the flux-flow solution, one finds that $\langle f_p(v)\rangle \propto 1/\sqrt{v}$. An extended intermediate-velocity regime $v_p < v < \kappa v_p$ appears

for large κ values where $\langle f_p(v)\rangle \propto 1/v$. This rapid decay is due to a collapse of the longitudinal pinning or trapping length $t_\parallel(v)$ from $\sigma\kappa$ to the geometrical pin size σ with increasing velocity v. Finally, developing a perturbative theory around the static (pinned) solution, we find a decreasing pinning force $\langle f_p(v)\rangle - f_c \propto -\sqrt{v}$ at small velocities $v < v_p$. This square-root *decrease* in the pinning force at small velocities v entails an interesting feature in the force-velocity characteristic; the latter exhibits hysteretic behavior with separated jumps [14] upon increasing/decreasing the drive F_L across F_c.

The pinning force $\langle f_p(v)\rangle$ looks different *when pinning is weak*. For $\kappa < 1$, the critical force $f_c = \langle f_p(v=0)\rangle$ vanishes and the dynamical force $\langle f_p(v)\rangle \propto \sqrt{v}$ increases with velocity. This behavior remains valid for moderately strong pinning with $\kappa \gtrsim 1$, where the critical current $f_c \propto (\kappa-1)^2$ assumes a finite value [17] and the small v correction $\langle f_p(v)\rangle - f_c \propto \sqrt{v}$ still increases with velocity v, see Fig. 6. This square-root *increase* in the pinning-force density then leads to a smooth and reversible quadratic onset of the velocity, $v \propto (F_\text{L} - F_c)^2$ in a narrow region above F_c.

The results at small $\kappa \ll 1$ can all be obtained with the help of perturbation theory which directly addresses the pinning-force density $\langle F_p(v)\rangle$. Thereby it turns out that the expression for the lowest-order correction $\langle F_p^{(1)}(v)\rangle$ has a form which is identical to that of weak collective pinning theory, after proper identification of the pinning-energy correlators. This also implies that we can use the single-pin analysis to rederive the weak collective pinning results for the critical current density j_c, a quite remarkable finding.

In the following, we first (Sec. II) derive the expression for the pinning-force density $\langle F_p(v)\rangle$, simplify the problem to a manageable version of the single-pin-single-vortex situation, and derive the Labusch criterion separating weak from strong pins. In Sec. III, we focus on the static solution and discuss the universal solution at very strong pinning $\kappa \gg 1$. Section IV is devoted to the dynamic solution at finite velocities. In order to get an insight into the problem, we first provide numerical results for the average pinning force $\langle f_p(v)\rangle$ generated by a Lorentzian-shaped pinning potential and identify the various strong pinning regimes at high, intermediate, and low velocities. We discuss the various analytical schemes to deal with the problem, perturbative methods at large and small velocities and a self-consistent universal solution in between. A special discussion is devoted to the transverse pinning or trapping length $t_\perp(v)$ and its velocity dependence, see Sec. IV E. In Sec. V, we discuss the excess-force characteristic as obtained in the dilute pin-density limit. Section VI is devoted to a brief discussion of model potentials, in particular, the (exactly solvable) parabolic potential, which is often used in the context of simulations on vortex dynamics in pinning landscapes [28]. In Sec. VII, we summarize our results and place them into context. A brief account on parts of this work has been given in Ref. [29].

II. FORMALISM

We assume a random homogeneous distribution of identical defects of density n_p and acting on the vortices with a pinning potential

$$\varepsilon_\text{p}(\mathbf{R},z) = e_p(\mathbf{R})\,\delta(z), \tag{4}$$

of depth e_p and width $\sigma \sim \xi \ll a_0$ [ξ and $a_0 = (\Phi_0/B)^{1/2}$ denote the coherence length or vortex core size and the distance between vortices, respectively]. The pinning force is given by the gradient $\mathbf{f}_p(\mathbf{R}) = -\nabla_\mathbf{R} e_p(\mathbf{R})$ and we denote its maximal amplitude by f_p. Defects, which strongly suppress the superconducting order parameter within a coherence volume $\sim \xi^3$, generate a pinning potential of depth $e_p \sim H_c^2\xi^3 \sim \varepsilon_0\xi$, with $\varepsilon_0 = (\Phi_0/4\pi\lambda)^2$ the vortex line energy. On the other hand, for small (atomic) defects [30], the pinning energy is of order $e_p \sim H_c^2\xi\sigma_\text{sc}$, with the electronic scattering cross section σ_sc replacing the larger area ξ^2; such defects then are more likely to be weakly pinning. An extensive discussion of different types of pinning defects including insulating and metallic defects and defects leading to a modulation of T_c and of the mean free path ℓ (termed δT_c and $\delta\ell$ pinning) have been presented in Ref. [19], including also the various H-T diagrams illustrating where pinnning is strong. Below, we will make occasional use of Lorentzian-shaped pinning potentials [29] $e_p(\mathbf{R}) = -e_p/(1 + R^2/\sigma^2)$ with $\sigma = \sqrt{2}\xi$ as motivated by the (variational) shape of the vortex core [31,32] in combination with a pointlike defect.

An ensemble of (homogeneously distributed) defects located at positions $\mathbf{r}_i = (\mathbf{R}_i, z_i)$ acts on the flux lines at the positions [33] $(\mathbf{R}_\mu + \mathbf{u}_\mu(z,t), z)$ with the pinning-force density (exploiting self-averaging)

$$\langle \mathbf{F}_p\rangle = -\frac{1}{N}\sum_\mu^N \int \frac{dz}{L}\,\mathbf{F}_p(\mathbf{r}_\mu,\mathbf{u}_\mu), \quad \text{with}$$

$$\mathbf{F}_p(\mathbf{r}_\mu,\mathbf{u}_\mu) = \frac{1}{a_0^2}\sum_i \mathbf{f}_p[\mathbf{R}_\mu + \mathbf{u}_\mu(z,t) - \mathbf{R}_i]\delta(z - z_i). \tag{5}$$

The minus sign in Eq. (5) derives from our sign convention in Eq. (1) where $\langle F_p\rangle$ acts against the direction of the drive. Here, the coordinates $\mathbf{r}_\mu = (\mathbf{R}_\mu, z)$ describe an ideal triangular Abrikosov lattice with density $a_0^{-2} = B/\Phi_0$ that is fixed in space. They serve as reference positions for the vortices that move with velocity $\mathbf{v}t$. The dynamical displacement field $\mathbf{u}_\mu(z,t) = \mathbf{v}t + \mathbf{u}_{p,\mu}(z,t)$ then involves two terms, the first describing their bulk average motion, while the pinning-induced term $\mathbf{u}_{p,\mu}(z,t)$ accounts for the vortex deformations away from the ideal lattice configuration. This definition of the displacement field differs from the one used in the static strong-pinning situation in Ref. [17], where the displacement field has been measured with respect to the free asymptotic positions of the (static) vortices.

The dynamical displacement field $\mathbf{u}_\mu(z,t)$ can be found from the self-consistent solution of the vortex equation of motion which we write in its integral form,

$$\mathbf{u}_\nu(z,t) = \mathbf{v}t + a_0^2\sum_\mu \int dz'dt'\,\hat{\mathbf{G}}(\mathbf{R}_\nu - \mathbf{R}_\mu, z - z', t - t') \times \mathbf{F}_p[\mathbf{r}'_\mu, \mathbf{u}_\mu(z',t')], \tag{6}$$

with $\mathbf{r}'_\mu = (\mathbf{R}_\mu, z')$. In the absence of pinning, the first term accounts for the Lorentz force in Eq. (1) generating the flux-flow velocity $\mathbf{v} = \mathbf{F}_\text{L}/\eta$; in the presence of a pinning-force density $\langle \mathbf{F}_p\rangle$, the velocity $\mathbf{v}$ has to be determined self-consistently from the dynamical equation (1). The dynamical elastic Green's function $\hat{\mathbf{G}}(\mathbf{r},t)$ is given by the Fourier transform of the matrix

[we define $\mathbf{k} = (\mathbf{K}, k_z)$]

$$G_{\alpha\beta}(\mathbf{k},\omega) = \frac{K_\alpha K_\beta/K^2}{c_{11}K^2 + c_{44}k_z^2 - i\eta\omega} + \frac{\delta_{\alpha\beta} - K_\alpha K_\beta/K^2}{c_{66}K^2 + c_{44}k_z^2 - i\eta\omega}, \tag{7}$$

with the dispersive elastic moduli [10] $c_{11}(\mathbf{k})$ (compression), $c_{44}(\mathbf{k})$ (tilt), and the nondispersive shear c_{66}, as well as the dissipative dynamical term $-i\eta\omega$.

For a dilute density n_p of pinning defects with moderately to strong pinning forces but trapping no more than one vortex at a time, we can reduce the sum over i in Eq. (5) and the sum over μ in Eq. (6) to only one term each; we call this the single-pin/single-vortex limit which will provide us with results correct to order n_p. With the vortex μ impinging on the defect at $(\mathbf{R_p}, z_p)$, we have to find the displacement field

$$u_{v,\alpha}(z,t) = v_\alpha t + \int dt'\, G_{\alpha\beta}(\mathbf{R}_v - \mathbf{R}_\mu, z - z_p, t - t') \times f_{p,\beta}[\mathbf{R}_\mu + \mathbf{u}_\mu(z_p,t') - \mathbf{R}_p]. \tag{8}$$

Once we have (self-consistently) solved the dynamical equation for the displacement field $u_{\mu,\alpha}(z_p,t)$,

$$u_{\mu,\alpha}(z_p,t) = v_\alpha t + \int dt'\, G_{\alpha\alpha}(0,t-t') \times f_{p,\alpha}[\mathbf{R}_\mu + \mathbf{u}_\mu(z_p,t') - \mathbf{R}_p], \tag{9}$$

we can find the full displacement field $u_{v,\alpha}(z,t)$ by simple integration of Eq. (8). In Eq. (9), we have used that the Green's function $G_{\alpha\beta}(\mathbf{r} = 0,t)$ is diagonal.

Next, we simplify the expressions for $\langle \mathbf{F}_p \rangle$ and $u_{\mu,\alpha}(z_p,t)$, Eqs. (5) and (9), in the single-pin-single-vortex approximation. We choose a representative vortex at $\mathbf{R}_\mu = \mathbf{R}$ and a pin at $\mathbf{r}_p$ and rewrite the average pinning-force density Eq. (5) in the form

$$\langle \mathbf{F}_p \rangle = -\frac{n_p}{N a_0^2 L} \int \frac{d^2R}{a_0^2} \int dz \int d^3r_p \times \mathbf{f}_p[\mathbf{R} - \mathbf{R}_p + \mathbf{u}(\mathbf{R} - \mathbf{R}_p, z, t)]\delta(z - z_p), \tag{10}$$

where we have replaced the sums over μ and i by the integrations over d^2R/a_0^2 and $n_p d^3 r_p$. We can choose the pin location $(\mathbf{R}_p, z_p)$ at the origin and cancel the integral over $\mathbf{r}_p$ against the volume $N a_0^2 L$ to arrive at

$$\langle \mathbf{F}_p(v) \rangle = -n_p \int \frac{d^2R}{a_0^2}\, \mathbf{f}_p[\mathbf{R} + \mathbf{u}(\mathbf{R},0,t)]. \tag{11}$$

Furthermore, we note that we can rewrite the displacement field in Eq. (9) in the form $\mathbf{u}(\mathbf{R},0,t) = \mathbf{v}t + \mathbf{u}_p(\mathbf{R} + \mathbf{v}t)$, where the pinning-induced part $\mathbf{u}_p$ of the displacement $\mathbf{u}$ obeys the equation

$$u_{p,\alpha}(\mathbf{R} + \mathbf{v}t) = \int dt'\, G_{\alpha\alpha}(0,t-t') \times f_{p,\alpha}[\mathbf{R} + \mathbf{v}t' + \mathbf{u}_p(\mathbf{R} + \mathbf{v}t')]. \tag{12}$$

The force in Eq. (11) can be written as $\mathbf{f}_p[\mathbf{R} + \mathbf{v}t + \mathbf{u}_p(\mathbf{R} + \mathbf{v}t)]$ and thus only depends on the combined argument $\mathbf{R} + \mathbf{v}t$, the distance between the vortex and the pin at time t.

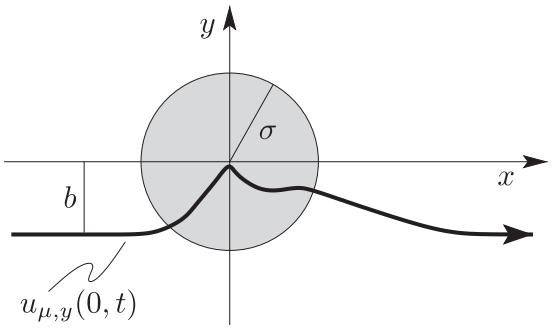

FIG. 2. Illustration of a vortex trajectory $\mathbf{u}_\mu(0,t)$ with a finite impact parameter $u_{\mu,y}(z = 0, t = -\infty) = -b$, approaching a defect with pinning potential of width σ located at $\mathbf{R}_p = (0,0)$; for a Lorentzian-shaped pinning potential, $\sigma = \sqrt{2}\xi$. For a strong pinning center, trapping and depinning are strongly asymmetric, which gives rise to a finite pinning force $\langle F_p(v) \rangle$.

Next, we simplify our task by considering a geometry (see Fig. 2) with impact parameter $b = 0$, i.e., a vortex hitting the pin head-on. The average pinning force for this situation can be written as [see Eq. (11)]

$$\langle f_p(v) \rangle \approx -\int \frac{dx}{a_0}\, f_p[x + vt + u_p(x + vt)]. \tag{13}$$

This expression can be further simplified, on the one hand, by selecting convenient references for the position x and the time t, on the other hand, by choosing between space and time averaging. Specifically, we change space to time average, $dx \to v dt$, and then set $x = 0$, what corresponds to choosing our reference position such that the unperturbed vortex passes the pin at time $t = 0$. Using $u(vt) = vt + u_p(vt)$, we arrive at the final result for the average pinning force

$$\langle f_p(v) \rangle \approx -\int \frac{dx}{a_0}\, f_p[u(x)], \tag{14}$$

where the displacement field $u(x = vt) = u_{\mu,x}(0,t)$ obeys the self-consistent dynamical equation Eq. (9) in the simplified form

$$u(x) = x + \int_{-\infty}^{x} \frac{dx'}{v}\, G[0,(x - x')/v]\, f_p[u(x')]. \tag{15}$$

In Eq. (15), we have made use of causality, forcing the Green's function to vanish at negative times $t - t' < 0$. The coordinate $x = vt$ denotes the asymptotic position of the vortex at $z = \pm\infty$ (replacing u by $u - x$ produces the displacement field defined in Ref. [17]) and we have used the simplified notation $G = G_{xx}$ and $f_p = f_{p,x}$ for the force along x.

In order to find the mean pinning-force density $\langle F_p(v) \rangle$, we have to perform an additional average over the impact parameter $b = y$ of the vortex on the pin in Eq. (11), see Fig. 2. This task is dealt with by equally treating all trajectories within the transverse trapping range $t_\perp(v)$ of the pin; this can be done exactly in the static limit [17], see below, and is a good approximation at finite velocities where $t_\perp(v)$ depends on v as discussed in Sec. IV E. As a result, the average over b contributes a factor $2t_\perp(v)/a_0$ and the y component of the force averages to zero. We then obtain the final expression for

the mean pinning-force density $\langle F_p(v)\rangle$ along x in the form

$$\langle F_p(v)\rangle \approx n_p \frac{2t_\perp(v)}{a_0}\langle f_p(v)\rangle. \tag{16}$$

Equations (14)–(16) together with the dynamical equation (1) define the simplified problem which now is amenable to a complete (numerical) solution.

The local dynamical Green's function $G(t) \equiv G_{xx}(\mathbf{r}=0,t)$ is obtained from the Fourier transform G_{xx} as given by Eq. (7). We neglect the compression modes as compared to the softer shear modes [10] to find (the average of K_y^2/K^2 over the Brillouin zone leads to the overall factor $1/2$, which has been ignored in Ref. [10])

$$G(t) = \Theta(t)\frac{1}{2\eta}\int_{\mathrm{BZ}} \frac{d^3k}{(2\pi)^3} e^{-[c_{66}K^2 + c_{44}(\mathbf{k})k_z^2]t/\eta}. \tag{17}$$

Depending on the time t, the integral is either cut by the exponential or by the Brillouin zone boundary (we use a circularized Brillouin zone with $K_{\mathrm{BZ}}^2 = 4\pi/a_0^2$); in addition, the dispersive nature of the tilt modulus has to be accounted for within an intermediate-time regime.

In the static limit, it is the local static elastic Green's function $G(\mathbf{r}=0,\omega=0) = \int_0^\infty dt\, G(0,t)$, which plays an important role; the latter defines an effective elasticity [19] through $\bar{C} = 1/G(0,0)$,

$$\bar{C} \approx 2\sqrt{2\pi \ln(a_0/\xi)}\frac{\varepsilon_0}{a_0}, \tag{18}$$

where $\varepsilon_0 = (\Phi_0/4\pi\lambda)^2$ denotes the characteristic line energy of a vortex. The above estimate derives from analyzing the deformation of a vortex trapped within a cage potential $V_{\mathrm{cage}} = \pi\varepsilon_0(u/a_0)^2$ set up by the neighboring vortices [19,34] and provides an upper limit for $\bar{C}$; a precise determination of $\bar{C}$ requires a numerical analysis. In the following, we drop the logarithmic factor.

The characteristic time separating different dynamical regimes is given by the thermal relaxation time

$$t_{\mathrm{th}} = \frac{\eta}{c_{66}K_{\mathrm{BZ}}^2} \approx \frac{4\eta a_0^3}{\sqrt{2\pi}\bar{C}}, \tag{19}$$

the dissipative relaxation time of free short-scale elastic deformations as induced, e.g., by thermal fluctuations [10]. At long times $t > t_{\mathrm{th}}(\lambda/a_0)^2$, the integral in (17) is cut by the exponential at small values of K such that the dispersion in c_{44} can be neglected; with $c_{44} \approx B^2/4\pi$ and $c_{66} \approx \Phi_0 B/(8\pi\lambda)^2$ one finds the 3D Green's function [10]

$$G^{\mathrm{3D}}[t_{\mathrm{th}}(\lambda/a_0)^2 \ll t]) \approx \frac{1}{2\sqrt{2}\pi}\frac{a_0/\lambda}{\bar{C}t_{\mathrm{th}}}\left(\frac{t_{\mathrm{th}}}{t}\right)^{3/2}, \tag{20}$$

describing a response $G^{\mathrm{3D}}(t) \propto t^{-d/2}$ involving the entire $d=3$ bulk vortex system. At intermediate times $t_{\mathrm{th}}(\lambda/a_0)^2 > t > t_{\mathrm{th}}$, the dispersion $c_{44} \approx B^2/4\pi\lambda^2K^2$ in the tilt modulus becomes relevant and the response is that of a dispersive elastic manifold with an elastic Green's function behaving as the one of a 4D nondispersive medium [10],

$$G^{\mathrm{4D}}[t_{\mathrm{th}} \ll t \ll t_{\mathrm{th}}(\lambda/a_0)^2] \approx \frac{1}{2\sqrt{2}}\frac{1}{\bar{C}t_{\mathrm{th}}}\left(\frac{t_{\mathrm{th}}}{t}\right)^2. \tag{21}$$

For short times $t < t_{\mathrm{th}}$, the integral is cut by the Brillouin-zone boundary. This short-time response describes the dynamics of an individual vortex line [10] (in this 1D limit both, longitudinal and transverse parts of the Green's function Eq. (7), contribute)

$$G^{\mathrm{1D}}(t \ll t_{\mathrm{th}}) \approx \Theta(t)\sqrt{\frac{2}{\pi}}\frac{1}{\bar{C}t_{\mathrm{th}}}\left(\frac{t_{\mathrm{th}}}{t}\right)^{1/2}. \tag{22}$$

Note that the time integral in Eq. (15) is well behaved as the Green's function is regular (integrable) at long times (since $G^{\mathrm{3D}} \propto t^{-3/2}$) as well as at short times (since $G^{\mathrm{1D}} \propto t^{-1/2}$), with the main contribution to the time integral originating from t_{th}.

Applicability

The formalism and the results derived in this paper apply in the 3D strong pinning regime of the pinning diagram in Ref. [17]. This density-force pinning diagram delineates the various regimes of vortex pinning into four domains, 3D weak pinning at small f_p and small/intermediate n_p, single vortex (or 1D) weak pinning at small/intermediate forces f_p and large densities n_p, 1D strong pinning at large f_p and intermediate n_p, and finally the region of interest in the present work with the condition of large force $f_p > \bar{C}\sigma$ and small density $n_p < \bar{C}/a_0\sigma f_p$. The strong pinning condition $f_p > \bar{C}\sigma$ guarantees, that defects induce bistable solutions with pinned and unpinned branches such that a single defect can pin a vortex. On the other hand, the low-density condition $n_p < \bar{C}/a_0\sigma f_p$ makes sure that the pinning action of defects do not interfere. Hence care has to be taken to properly interpret the term "strong" pinning, as it does *not* imply a high critical current density close to the depairing current density due to the low defect density. Strong pinning in the sense of large j_c requires large forces f_p *and* large densities n_p, what naturally takes us across the line $n_p f_p \sim \bar{C}/a_0\sigma$ and into the 1D strong pinning domain. Similarly, decreasing the magnetic field at fixed pinning force f_p and defect density n_p takes us across the 3D-1D strong pinning boundary as B decreases below $(n_p\xi^3)(f_p/\varepsilon_0)H_{c2}$.

Another limitation of our analysis is given by the condition that the maximal displacement $u \sim \kappa\sigma$ before depinning should be smaller than the intervortex separation a_0, $\kappa\sigma < a_0$. Indeed, as $u \sim \kappa\sigma$ approaches a_0, the angle $\partial_z u \sim u/a_0$ enclosed by the vortex pinned to the defect approaches unity and our elastic theory breaks down. Furthermore, the periodicity of the pinning landscape induced by the lattice period cannot be ignored any more [19]. This condition then limits the strength f_p of the defects: using $\kappa \sim f_p/\bar{C}\sigma$ (see below), we find that the pinning force f_p of individual defects should satisfy the constraint $f_p < \bar{C}a_0$. Using the above estimate for $\bar{C}$, we find that $f_p < \varepsilon_0$. Superstrong pins with pinning forces f_p beyond this value induce large plastic deformations as described by Schönenberger *et al.* [35], where finite segments of line- or columnar pins have been considered. Depinning from such defects then can proceed via vortex recombination or loop formation, limiting the maximally possible force f_p that a defect can exert on a vortex. Also, we note that 'strong' pinning is often associated with defects of special geometric shape, e.g., columnar pins or grain/twin boundaries that pin vortices as a line object rather than in a point. Such *correlated* pinning has been extensively discussed in Ref. [10], see also Ref. [36]

for recent computational work, and is not explicitly considered in the present analysis. Although the above restriction on f_p limits the applicability of our analysis in the strict sense, we believe that the important result regarding the separation of velocity scales and the resulting excess-current characteristic remain valid.

III. STATIC SOLUTION

The critical pinning-force density F_c is obtained in two steps, where in the first, we determine the pinning-force average f_c (longitudinal average) and in the second, we find the transverse trapping length $t_\perp$ (transverse average).

A. Longitudinal average f_c

In the static situation, the self-consistent integral equation (15) turns into the simpler algebraic equation

$$u_s(x) = x + f_p[u_s(x)]/\bar{C}. \tag{23}$$

Solving Eq. (23) self-consistently for $u_s(x)$ and inserting the result into Eq. (14), we obtain the critical force

$$f_c = \langle f_p(v=0)\rangle = -\int \frac{dx}{a_0} f_p[u_s(x)]. \tag{24}$$

The static self-consistency equation (23) can be derived from a total energy $e_t(x)$ that includes both the elastic energy of the vortex deformation and its pinning energy, see Fig. 3(d),

$$e_t(x) \equiv e_t[x; u_s(x)] = \frac{\bar{C}}{2}[u_s(x) - x]^2 + e_p[u_s(x)]. \tag{25}$$

Indeed, minimising $e_t(x;u)$ with respect to u, $\partial_u e_t(x;u) = \bar{C}(u-x) - f_p(u) = 0$, reproduces Eq. (23). Then, the total derivative of $e_t(x)$ can be written in the form

$$\frac{de_t(x)}{dx} = -\bar{C}(u_s - x) + \partial_x u_s[\bar{C}(u_s - x) - f_p(u_s)]$$

and using Eq. (23), we find that

$$f_p[u_s(x)] = -\frac{de_t(x)}{dx}. \tag{26}$$

This relation is very helpful in evaluating the critical force f_c in Eq. (24). At weak pinning, the effective static pinning force $f_p[u_s(x)]$ appearing in Eq. (24) is a single-valued smooth function, resulting in a vanishing force average:

$$f_c = \int \frac{dx}{a_0}\frac{de_t(x)}{dx} = \frac{e_t(\infty) - e_t(-\infty)}{a_0} = 0. \tag{27}$$

A finite critical force density $F_c \propto n_p^2$ then is established through fluctuations in the defect density as described through weak collective pinning theory.

A strong pin producing a finite average pinning-force density $\propto n_p$ is characterized by the appearance of bistable solutions (or branches) in the single-pin problem Eq. (23). The critical force f_c then depends on the occupation of these branches by vortices, with an asymmetric occupation of the solutions resulting in a finite average force. Indeed, when typical values of $f_p/\sigma\bar{C}$ become large, the bare pinning force $f_p(x)$, see inset of Fig. 3(c), when evaluated at the shifted position $u_s(x)$, is tilted backward, see Fig. 3(c). In

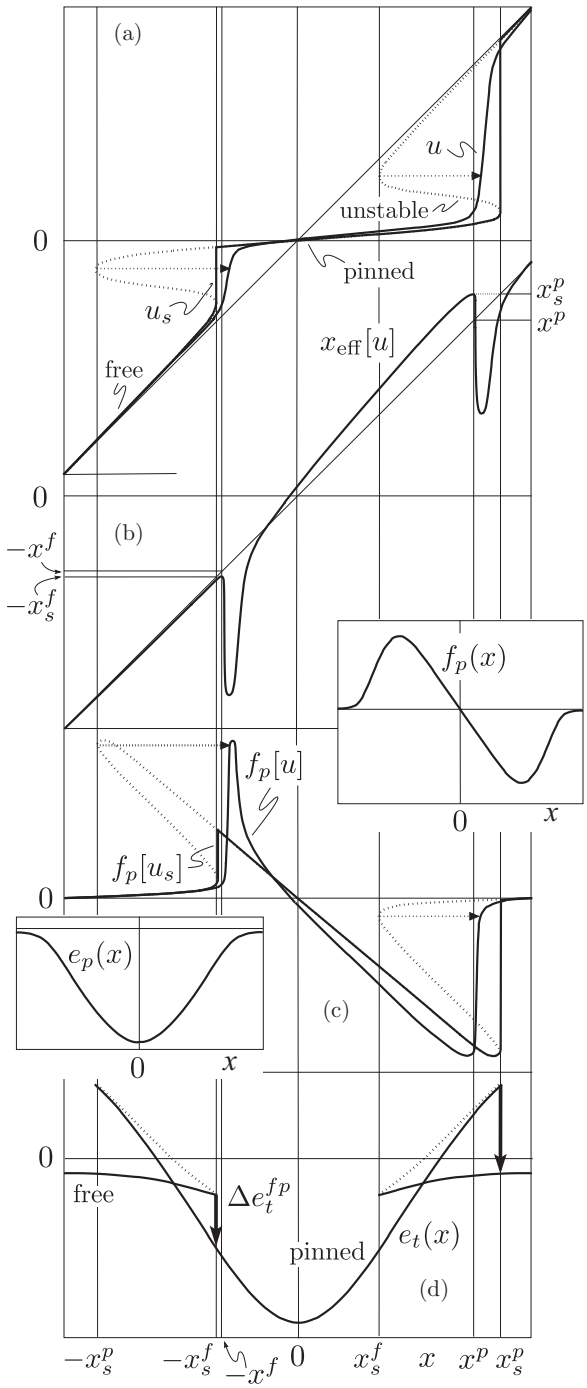

FIG. 3. Sketch of the static and dynamic displacement fields $u_s(x)$ and $u(x)$ (a). The static displacement $u_s(x)$ jumps from the free to the pinned branch at $-x_s^f$ and back to the free branch at x_s^p. For the smooth dynamic displacement $u(x)$, these jumps are replaced by steep rises at the shifted positions $-x^f$ and x^p. Below, we will make use of a smooth multivalued static solution $\bar{u}_s$ where the jumps are replaced by the unstable branch u_s^u (dotted). The dotted arrows refer to the shift $x_{\rm eff}[u](x)$, see (b), that connects the smooth static and dynamic solutions $\bar{u}_s(x)$ and $u(x)$, respectively. (b) Effective coordinate $x_{\rm eff}[u](x) = x - \delta x[u](x)$ allowing to express the dynamic solution through the static one, $u(x) = \bar{u}_s[x_{\rm eff}[u](x)]$. (c) Static and dynamic force profiles $f_p[u_s(x)]$ and $f_p[u(x)]$. (d) Static total energy profile $e_t(x)$. The insets show the bare force and energy profiles of the pinning center.

this strong-pinning situation the derivative

$$\partial_x u_s(x) = \frac{1}{1 - \partial_{u_s} f_p[u_s(x)]/\bar{C}} \tag{28}$$

diverges at the positions $\pm x_s^f$ and $\pm x_s^p$ where $\partial_{u_s} f_p[u_s(x)] = \bar{C}$, signaling the appearance of multiple solutions with pinned $[u_s^p(x)]$, unstable $[u_s^u(x)]$, and free $[u_s^f(x)]$ or unpinned branches, see Fig. 3. Strong pinning then requires the ratio

$$\kappa = \max_x \left\{\partial_{u_s} f_p[u_s(x)]\right\}/\bar{C} = \max_x [f_p'(x)]/\bar{C} \tag{29}$$

to be larger than one, $\kappa > 1$; this is the famous Labusch criterion for strong pinning [6]. A vortex incident from the left onto the defect and moving towards the right will leave the free branch $u_s^f(x)$ at $-x_s^f$ and jump to the pinned branch $u_s^p(x)$ [see Fig. 3(a), the unstable branch $u_s^u(x)$ and parts of the pinned branch are jumped over]. After crossing the defect, the vortex will depin from the pinned branch at x_s^p and jump back to the free branch (the points x_s^f and $-x_s^p$ are relevant when the vortex moves from right to left). As a result, the critical pinning force f_c becomes finite and equal to the sum of energy jumps at $-x_s^f$ and x_s^p,

$$f_c = \left[\int_{-\infty}^{-x_s^f} + \int_{-x_s^f}^{x_s^p} + \int_{x_s^p}^{\infty}\right] \frac{dx}{a_0} \frac{de_t(x)}{dx} = \frac{\Delta e_t^{fp} + \Delta e_t^{pf}}{a_0} \tag{30}$$

with the positive jumps $\Delta e_t^{fp} = e_t^f(-x_s^f) - e_t^p(-x_s^f)$ and $\Delta e_t^{pf} = e_t^p(x_s^p) - e_t^f(x_s^p)$. Hence it is the asymmetry between jumping into the pinning well at $-x_s^f$ and out of it at x_s^p which generates the finite (and actually maximal) pinning force [6,8,14,17] f_c, see Fig. 3(c). Alternatively, Eq. (30) may be interpreted in a (nonequilibrium) statistical sense in terms of an imbalance between the occupation of the different pinning branches that is produced by the applied Lorentz force.

B. Trapping lengths $t_\perp$ and $t_\parallel$

In order to obtain the critical force density F_c, we have to determine the trapping length $t_\perp$, see Eq. (16). For a radially symmetric defect potential, this is conveniently done by considering the total energy $e_t(R;r)$ for a vortex with radial asymptotic and tip positions R and r, see Eq. (25),

$$e_t(R;r) = \frac{\bar{C}}{2}(r - R)^2 + e_p(r). \tag{31}$$

Plotting this function at fixed R versus r, one observes a single (pinned) minimum in the variable r for $0 < R < R_s^f$, two minima (pinned and free) when $R_s^f < R < R_s^p$, and again a single (free) minimum for $R > R_s^p$, see Fig. 4; these minima determine the (static) tip position $r_s(R)$ at given asymptotic position R; indeed, the condition $\partial_r e_t(R;r) = 0$ at fixed R reproduces Eq. (23) in the form $r = R + f_p(r)/\bar{C}$ and interrelates asymptotic (R) and tip (r) positions of the vortex. The appearance or disappearance of these minima at $R_s^f (= x_s^f)$ and $R_s^p (= x_s^p)$ signals the beginning or ending of the free and pinned branches. At these points, the second derivative $\partial_r^2 e_t(R;r) = 0$ vanishes as well, i.e., the curvatures in the elastic and pinning term of Eq. (31) compensate

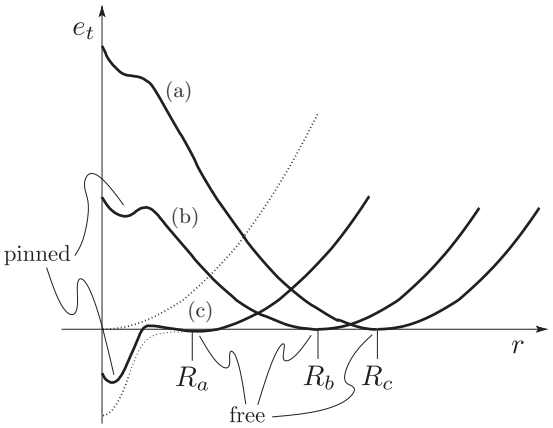

FIG. 4. Total energy $e_t(R;r)$ providing the configurational energy of a vortex at the asymptotic distance R from the pin when its tip resides at the distance r. Minimizing $e_t(R;r)$ at fixed R with respect to r defines the static tip position $r_s(R)$. Dotted lines trace the pinning potential $e_p(r)$ and the elastic energy $\bar{C}r^2/2$. Solid lines show the situation for (a) $R_s^f < R = R_a < R_s^p$ with two minima, just before the vortex in the free minimum jumps into the pin at $R_s^f = x_s^f$, (b) $R_s^f < R = R_b < R_s^p$ with two minima just before depinning at $R_s^p = x_s^p$, and (c), $R = R_c > R_s^p$ with one (free) minimum just after depinning at R_s^p.

and hence

$$\partial_r f_p(r)|_{r(R_s^{f,p})} = \bar{C}. \tag{32}$$

The latter condition actually determines the critical tip positions $r_s^f = r(R_s^f)$ and $r_s^p = r(R_s^p)$, while the corresponding asymptotic positions R_s^f and R_s^p are obtained from solving the force balance equation $r = R + f_p(r)/\bar{C}$.

In the static situation, a vortex approaching the defect gets trapped as soon as it enters the circle at R_s^f: as the free branch ends at R_s^f, the vortex tip falls into the stable minimum at $r(R_s^f)$, which resides on the pinned branch, see curve a) in Fig. 4. Hence all vortices impacting the defect within a distance R_s^f will get trapped and we find that

$$t_\perp = R_s^f = x_s^f, \tag{33}$$

see also Ref. [17]. Similarly, the vortices remain trapped by the pin until the asymptotic position R_s^p is reached and we obtain the longitudinal trapping length

$$t_\parallel = R_s^p = x_s^p. \tag{34}$$

Hence the positions $\pm x_s^f$ and $\pm x_s^p$, where the slope $\partial_x u_s(x)$ of the static displacement diverges, also determine the physical lengths $t_\perp$ and $t_\parallel$ where the vortices get and remain trapped, respectively. Finally, we combine the results Eq. (30) for the critical pinning force and Eq. (33) for the transverse trapping length into the expression for the critical-force density F_c, see Eq. (16), and obtain

$$F_c = \frac{2x_s^f}{a_0^2} n_p \left(\Delta e_t^{fp} + \Delta e_t^{pf}\right). \tag{35}$$

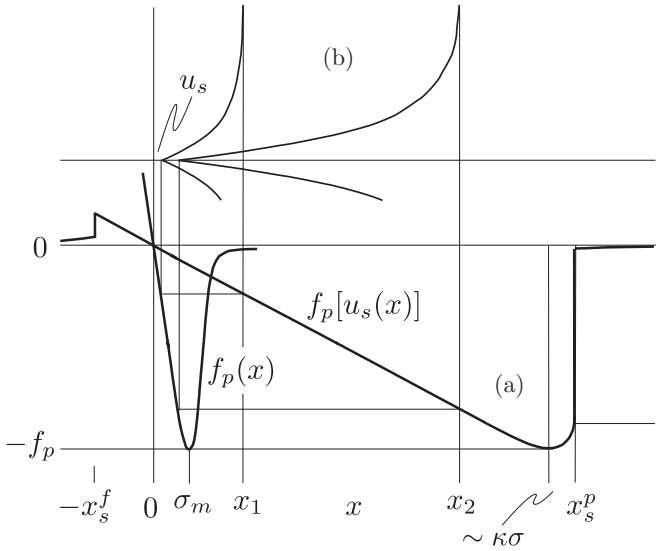

FIG. 5. (a) Bare and effective static pinning forces $f_p(x)$ and $f_p[u_s(x)]$ for a strong pinning potential. The steep negative slope $\partial_x f_p(x)$ on the scale σ transforms into the flat universal slope $-\bar{C}x$ in $f_p[u_s(x)]$ on the larger scale $\kappa\sigma$. The rounding before the collapse of $f_p[u_s(x)]$ at x_s^p extends over a distance $\sigma/2\kappa$ with a drop in restoring force $f_p/2\kappa^2$ and hence disappears in the limit $\kappa \to \infty$; the jump $\sim f_p/\kappa$ into the pin at $-x_s^f$ is small at large κ. (b) Vortex deformation for two asymptotic positions x_1 and x_2. While $x_2 - x_1$ increases on the scale $\kappa\sigma$ the associated displacements u_{s1} and u_{s2} change on the scale σ.

C. Universal static solution for very strong pinning $\kappa \gg 1$

It turns out, that the above general considerations can be pushed further in the limit of very strong pinning $\kappa \gg 1$, where a universal solution is available that is independent of the details of the pinning potential shape. We start from Eq. (23) by noticing that for the pinned situation, the last term $f_p[u_s(x)]/\bar{C}$ is large and has to be compensated by the coordinate x, since the tip position $u_s(x)$ on the right has to stay within the pin and hence is small, $u_s(x) < \sigma$. As a result, we find that for very strong pinning, the static force

$$f_p[u_s(x)] \approx -\bar{C}x \tag{36}$$

changes linearly over a wide range until reaching the largest (negative) force $-\bar{C}x_s^p \approx -f_p$ before depinning, see Fig. 5. The latter condition provides an accurate estimate for x_s^p in the very strong pinning limit,

$$t_\parallel = x_s^p \approx \frac{f_p}{\bar{C}} \sim \kappa\sigma. \tag{37}$$

Since $\kappa\sigma$ is large, the residual force after depinning is very small. Alternatively, the above result can be found by transforming Eq. (28) to its force analog; taking the derivative of Eq. (23) and using Eq. (28), we find that

$$\frac{df_p[u_s(x)]}{dx} = -\frac{\bar{C}}{1 - \bar{C}/\partial_u f_p[u_s(x)]}. \tag{38}$$

Again, for strong pinning, we have $\partial_u f_p[u_s(x)]/\bar{C} \gg 1$ over a large range $\sim\kappa\sigma$ along the x axis and hence the force derivative is renormalized to the (constant) effective elasticity $\bar{C}$, see Fig. 5.

Next, we discuss the jumps into and out of the pin at $-x_s^f$ and at x_s^p–we will need these results later in the discussion of the small velocity corrections to F_c. We distinguish pins with (long) tails decaying algebraically with $e_p(r) \propto (\sigma/r)^n$, from compact pins with tails decaying faster than any power; while this keeps our discussion more general, we may consider a situation in superconductors with small Ginzburg-Landau parameter where $\sigma \sim \xi \sim \lambda$ such that $e_p(r) \propto e^{-r/\sigma}$.

The jumps in and out of the pin are determined by the conditions $\partial_u e_t(x;u) = 0$ and $\partial_u^2 e_p(x;u]) = 0$, see Sec. III B. For the jump into the pin, we solve $\partial_u f_p(u) = \bar{C}$, cf. Eq. (32), and find that $u_s(-x_s^f) \sim -\kappa^{1/(n+2)}\sigma$ for a pin with tails and $u_s(-x_s^f) \sim -\sigma \ln\kappa$ for a compact pin. The associated asymptotic vortex position x_s^f follows from Eq. (23); since the jump into the pin takes place at small forces, we can approximate $-x_s^f \approx u_s(-x_s^f)$ and hence

$$t_\perp = x_s^f \sim \kappa^{1/(n+2)}\sigma \tag{39}$$

for a pin with tails. Similarly, for a compact pin, $x_s^f \sim \sigma \ln\kappa$. The result for the vortex jumping out of the pin has been found above, see Eq. (37).

The pinning force at $-x_s^f$ can be estimated with the help of Eq. (23): just before the jump, $u_s \approx -x_s^f$ and the force assumes a small value $f_p(-x_s^f) \approx f_p/\kappa^{(n+1)/(n+2)}$, while after the jump, $|u_s| \ll x_s^f$ and hence $f_p(u_s) \approx \bar{C}x_s^f \sim f_p\kappa^{1/(n+2)-1}$, which is of the same order. For a compact pin, the force before the jump is f_p/κ and assumes a logarithmically larger value after the jump, $(f_p/\kappa)\ln\kappa$. When jumping out of the pin, $u_s(x_s^p) \approx \sigma$ and the pinning force goes from $-f_p$ before the jump to very small values thereafter, $\sim -f_p/\kappa^{n+1}$ and $-f_p e^{-\kappa}$ for pins with tails and for compact pins, respectively.

The integration over the static force profile $f_p[u_s(x)]$ provides us with a critical force density [see Eqs. (24) and (33); note that $f_p[u_s(x)] \approx -\bar{C}x$ on the pinned branch]

$$\begin{aligned} F_c &\approx -n_p \frac{2x_s^f}{a_0^2} \int_{-x_s^f}^{x_s^p} dx\, f_p[u_s(x)] \\ &\approx \left(\frac{x_s^f + x_s^p}{a_0}\right)^2 n_p x_s^f \bar{C} \sim \frac{\kappa\sigma x_s^f}{a_0^2} n_p f_p, \end{aligned} \tag{40}$$

where we have used $x_s^p \sim \kappa\sigma \gg x_s^f$ and $\kappa \sim f_p/\sigma\bar{C}$ in the last estimate. The result involves, besides the maximal force f_p and density n_p of pins, the trapping area [15,17]

$$S_{\rm trap} = 2t_\perp t_\parallel \sim 2x_s^f\,\kappa\sigma. \tag{41}$$

With $\kappa \sim f_p/\sigma\bar{C}$ and $\bar{C} \sim \varepsilon_0/a_0$, see Eqs. (29) and (18), we obtain a field dependence $F_c \propto B^{(n+1)/2(n+2)}$ for the critical force F_c, assuming a pin with tails [15]. For large n, this produces the typical strong-pinning field-dependence $j_c \propto 1/\sqrt{B}$ for the critical current density, which is cutoff at small fields when bulk 3D strong pinning crosses over to single-vortex 1D strong pinning at $n_p a_0 \sigma^2 \kappa \sim 1$ [17]. Corrections to this universal static solution are discussed in Appendix A.

D. Static solution for moderately strong pinning $\kappa \gtrsim 1$

A similarly accurate analysis can be done at moderate pinning with $\kappa \gtrsim 1$ close to unity [17]. Expanding the pinning potential $e_p(x)$ around the point σ_{mc} of maximal negative curvature, $e_p''(x) = -\bar{C}\kappa + \alpha(x-\sigma_{mc})^2/2$, the transition to weak pinning can be described within the Landau formulation of a magnetic phase transition and one finds the result [17]

$$F_c \approx 18\frac{x_s^f}{a_0^2} n_p \frac{\bar{C}^2}{e_p''''}(\kappa-1)^2 \sim \frac{\sigma x_s^f}{a_0^2} n_p f_p (\kappa-1)^2, \qquad (42)$$

with $e_p''''|_{\sigma_{mc}} = \alpha$. In the last relation, we have used the estimate $\alpha \sim f_p/\sigma^3$ and $\bar{C}^2/\alpha \sim f_p\sigma$ with κ close to unity.

IV. DYNAMIC SOLUTION

Once the Lorentz force density F_L in Eq. (1) increases beyond the critical force F_c, the mean velocity v becomes finite. According to Eq. (15), the deformation $u(x)$ of the vortex is determined by the pinning force $f_p[u(x')]$ averaged over (past) times $t' = x'/v$ and weighted by the local dynamical Green's function $G(0,(x-x')/v)$. The average pinning force $\langle f_p(v)\rangle$, Eq. (14), then depends on the mean velocity v, starting at f_c for $v = 0$ and vanishing at large velocities v as the pins only weakly disturb the fast flow of vortices. Given the thermal time scale $t_{\rm th}$ of $G(0,t)$ and the pinning scale $\kappa\sigma$ over which the force $f_p[u(x')]$ remains finite, we can estimate the pinning velocity

$$v_p = \frac{\kappa\sigma}{t_{\rm th}} \sim \frac{f_p}{\eta a_0^3}, \qquad (43)$$

where dynamical effects start to modify $\langle f_p(v)\rangle$. The last expression describes the typical velocity scale of a vortex segment of length a_0 (the vortex tip) moving in the pinning potential $e_p(r)$, $\eta_l a_0 \dot{r} \sim f_p$ and $\eta_l = a_0^2\eta$ the line viscosity of a vortex.

Given the form of the pinning potential $e_p(r)$, the straightforward integration of the dynamical equation (15) gives us access to the average pinning force $\langle f_p(v)\rangle$ for any velocity v and the calculation of $t_\perp(v)$ provides us with the pinning-force density $\langle F_p(v)\rangle$ via Eq. (16). Analytic results, instead, have to be obtained using different approaches that depend on the velocity v: At high velocities, we use perturbation theory away from flux flow and directly address the force density $\langle F_p(v)\rangle$, in the intermediate velocity regime that is present at large values of κ, we determine the average force $\langle f_p(v)\rangle$ via construction of a self-consistent solution for $f_p[u(x)]$, while at low velocities, we find again the average $\langle f_p(v)\rangle$ using a perturbative approach, this time away from the static solution. The intermediate and small velocity results then have to be completed with a calculation of $t_\perp(v)$.

A. Overview on pinning-force averages

We first present the results obtained from a numerical forward integration of Eq. (15) for a Lorentzian-shaped pinning potential (we assume nondispersive moduli corresponding to a field $B \sim \Phi_0/\lambda^2$). In Fig. 6, we show the scaled average pinning force $\langle f_p(v)\rangle a_0^2/e_p\sigma$ versus the scaled velocity v/v_p. Varying the pinning energy e_p at fixed size σ, we follow

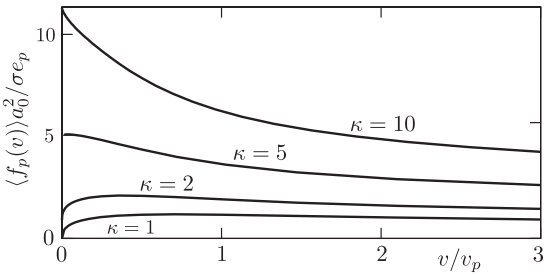

FIG. 6. Velocity dependence of the pinning-force density $\langle f_p(v)\rangle$ for Lorentzian pins $e_p(r) = -e_p/(1+r^2/\sigma^2)$ with Labusch parameters ranging from $\kappa = 1$ to $\kappa = 10$; the typical depinning velocity scale v_p where the pinning force changes depends on the Labusch parameter κ. We haven chosen a field $B = \Phi_0/\lambda^2$, $a_0 = \lambda$, such that the elastic moduli are nondispersive. While the pinning force decreases monotonically for large κ, it first increases at small velocities for $\kappa \gtrsim 1$ before eventually decreasing at large velocities. Original figure published in Ref. [29].

the evolution of the average pinning force $\langle f_p(v)\rangle$ from very strong pinning $\kappa = 10$ to moderately strong pinning at $\kappa \gtrsim 1$. With $e_p \sim H_c^2\xi^3 \sim \varepsilon_0\xi$ (H_c the thermodynamic critical field) the Labusch parameter can naturally access large numbers $\kappa \sim f_p/\sigma\bar{C} \sim (e_p/\sigma\varepsilon_0)(a_0/\sigma) \sim a_0/\xi \gg 1$. For very strong pinning, the critical force $f_c = \langle f_p(v=0)\rangle$ is large and the pinning force $\langle f_p(v)\rangle$ decreases when vortices start moving. On approaching the Labusch point $\kappa = 1$ and for weak pinning ($\kappa < 1$, not shown) the critical force vanishes and $\langle f_p(v)\rangle$ increases with v; this increase is trivially understood as the pinning force cannot turn negative. The vanishing of f_c on approaching $\kappa = 1$ follows a quadratic behavior [6,17], $f_c \propto (\kappa-1)^2$, see (42).

In order to understand the rough functional form of $\langle f_p(v)\rangle$ at small and large velocities v, we start from Eq. (14) and expand it about the static ($u_s(x)$) and dynamic ($u(x) \approx x = vt$) solutions of Eq. (15), respectively. In the static limit $v = 0$, $f_p[u_s(x')]$ can be taken out of the integral in Eq. (15); the remaining integral draws its main contribution from times $t \sim t_{\rm th}$, $\int dt\, G \sim t_{\rm th}\, G^{\rm 1D}(t_{\rm th}) \sim 1/\bar{C}$, see Eq. (22). The velocity correction at small v then derives from cutting this time integral at large but finite times $t_v \sim \kappa\sigma/v$, as the pinning force $f_p[u(x' = vt')]$ vanishes when the vortex leaves the pin at t_v. For $t_v > t_{\rm th}$ or $v < v_p$, the integral still picks up its main contribution near $t_{\rm th}$ that produces the static displacement $u_s(x)$; the correction $\int_{t_v}^{\infty} dt\, G^{\rm 3D}(t) \sim \sqrt{vt_{\rm th}/\kappa\sigma}/\bar{C}$ scales with $\sqrt{v/v_p}$ and hence $\langle f_p(v)\rangle - f_c \propto \sqrt{v/v_p}$ at small velocities. Note that a more refined discussion (see Sec. IV D below) is required in order to explain the sign change in the derivative of $\langle f_p(v\to 0)\rangle$ with decreasing κ, see Fig. 6.

In the limit of very high velocity v, the displacement $u(x) \approx vt$ and the force (14) vanishes since $\int dx f_p(x) = 0$. Corrections derive from the second term in Eq. (15), where the time integral now is cut on $t_v \sim \sigma/v \ll t_{\rm th}$. This implies that the entire pinning force derives from the integral at short times, $\int_0^{t_v} dt\, G^{\rm 1D}(t) \sim \sqrt{\sigma/vt_{\rm th}}/\bar{C}$, and hence the pinning force vanishes as $\langle f_p(v)\rangle \propto \sqrt{v_p/v}$, resulting in a monotonic decrease of $\langle f_p(v)\rangle$ for large values of κ. For small values of κ, i.e., $\kappa \to 1$, the vanishing of the critical force

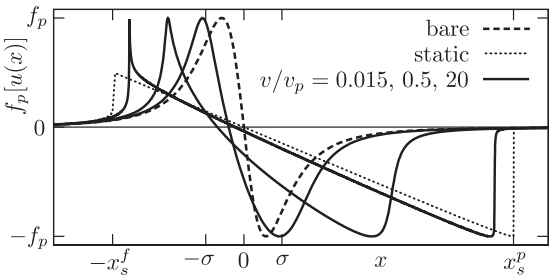

FIG. 7. Velocity dependence of the effective pinning force $f_p[u(x)]$ for a Lorentzian pin [with maximal force $f_p = (3\sqrt{3}/8)e_p/\sigma$] with Labusch parameter $\kappa = 5$ and for velocities $v/v_p = 0.015$, 0.5, and 20. The dynamical force profile is compared to the bare force $f_p(x)$ (dashed) and the static effective force $f_p[u_s(x)]$ (dotted). For small velocities, the finite-velocity solution follows closely the static solution $u_s(x)$, motivating an approximative scheme based on the latter as a starting point. For large velocities, the force profile approaches that of the bare force, motivating the use of perturbation theory around free flux flow.

$f_c = \langle f_p(v=0)\rangle \propto (\kappa-1)^2$ implies first an increase of the pinning-force density $\langle f_p(v)\rangle - f_c \propto \sqrt{v/v_p}$ at small v, which is later followed by the decrease $\propto \sqrt{v_p/v}$ at large v, resulting in the nonmonotonic behavior of $\langle f_p(v)\rangle$ shown in Fig. 6.

In the above very high velocity regime, the pinning-induced correction $u_p \sim f_p\sqrt{\sigma/vt_{\rm th}}/\bar{C} \sim \sigma\sqrt{\kappa v_p/v}$ should be small, $u_p < \sigma$, and thus $v > \kappa v_p$. This leaves a large intermediate velocity regime $v_p < v < \kappa v_p$ where neither of the above perturbative approaches can be applied. Understanding this intermediate velocity regime requires a more elaborate analysis of Eq. (15). Within this region, the two terms on the right are large and nearly compensate one another to produce a tip position $u(x) \lesssim \sigma$ within the pin. Hence Eq. (15) can be written in the form

$$-vt \approx \int_{-\infty}^{t} dt' G(0,t-t') f_p[u(t)], \tag{44}$$

where we have replaced space by time coordinates. Using the 1D Green's function (22), we estimate the right hand side as $\sqrt{t/t_{\rm th}}f_p[u(t)]/\bar{C}$ and therefore $f_p[u(t)] \sim -v\sqrt{t\,t_{\rm th}}\bar{C}$. The linear static force $f_p[u_s(x)] \approx -\bar{C}x$ of Eq. (36) then transforms into a square-root dynamic force

$$f_p[u(x)] \sim -\bar{C}\sqrt{x\sigma}\sqrt{v/v_\sigma}. \tag{45}$$

The maximal pinning force $-f_p$ is reached at $x \sim \kappa\sigma(v_p/v)$, reduced by a factor v_p/v with respect to the maximal pinning length $x_s^p \sim \kappa\sigma$ at vanishing velocity. The above results smoothly interpolate between those found in the small and large velocity regions at $v < v_p$ and $v > \kappa v_p$, respectively. Furthermore, one easily convinces oneself that the pinning time $t_v \sim \kappa\sigma v_p/v^2 < t_{\rm th}$ within this velocity region, justifying the use of the 1D Green's function. Integrating the pinning force (45) over the reduced pinning length $t_\parallel \kappa\sigma\sqrt{v_p/v}$, we obtain a decaying average pinning force $\langle f_p(v)\rangle \propto v_p/v$.

The above results provide a good qualitative understanding of the velocity dependence of the effective pinning force $f_p[u(x)]$ shown in Fig. 7 as calculated for a fixed Labusch parameter $\kappa = 5$ and different velocities v. Indeed, one finds that at low and high velocities v, the effective dynamical force smoothly evolves out of the static force $f_p[u_s(x)]$ (dotted in Fig. 7) and the bare force $f_p(x)$ (dashed in Fig. 7). Furthermore, at intermediate velocities, the effective pinning force roughly follows a square-root shape of reduced extent, in agreement with the result (45). The average pinning force $\langle f_p(v)\rangle$ shown in Fig. 6 derives from an average over the local pinning force $f_p[u(x)]$, see Eq. (16). In the following, we present a more detailed analysis of the various pinning and velocity regimes.

B. Perturbation theory around flux flow

When the effect of pinning is small, either at small $\kappa \ll 1$ or at high velocities v, we can use perturbation theory away from flux flow [10,20,21]. This analysis can be done on the full two-dimensional problem at $z = 0$, using the ansatz $\mathbf{u}(\mathbf{R},t) = \mathbf{v}t + \mathbf{u}_p(\mathbf{R}+\mathbf{v}t)$ for the dynamical displacement field with the pinning contribution $\mathbf{u}_p$ providing a small correction. We start with Eq. (12) and expand the pinning force in $\mathbf{u}_p$ to obtain the correction

$$u_{p,\alpha}(\mathbf{R}+\mathbf{v}t) \approx \int_{-\infty}^{t} dt' G[0,(t-t')] f_{p,\alpha}(\mathbf{R}+\mathbf{v}t'). \tag{46}$$

Next, we insert this expression back into the formula for the average pinning force density Eq. (11) (we assume a drive along x with $\mathbf{v} = (v,0)$ and evaluate the average force at $t = 0$) and arrive at

$$\langle F_p(v)\rangle \approx -n_p \int \frac{d^2R}{a_0^2}\,\partial_\alpha f_{p,x}(\mathbf{R}) \times \int_0^\infty dt\, G(0,t)\, f_{p,\alpha}(\mathbf{R}-\mathbf{v}t). \tag{47}$$

This result can be brought to the form known from weak collective pinning theory,

$$\langle F_p(v)\rangle \approx \int_0^\infty dt\, G(0,t)\, K^{x\alpha\alpha}(\mathbf{v}t) \tag{48}$$

with the pinning energy correlator

$$K(\mathbf{u}) = n_p \int \frac{d^2R}{a_0^2}\, e_p(\mathbf{R})\, e_p(\mathbf{R}-\mathbf{u}) \tag{49}$$

and the superscripts in Eq. (48) denoting derivatives with respect to u_x and u_α (and summation over $\alpha = x,y$). For weak pinning, the result Eq. (48) can be used for any velocity v.

1. Weak pins, small v

We first show that the pinning force indeed increases $\propto\sqrt{v}$ at small velocities. This is easily done in Fourier space, which takes Eq. (48) into the form (we assume a drive along x)

$$\langle F_p(v)\rangle \approx \frac{n_p}{a_0^2}\int \frac{d^2K}{(2\pi)^2}\, K^2 K_x\, |e_p(\mathbf{K})|^2 \times \int_0^\infty dt\, G(0,t)\sin(K_x v t). \tag{50}$$

Using the 3D Green's function Eq. (20) that is relevant at small velocities v, we obtain the result [with the numerical $\nu^< \approx K(1/2)/(3\sqrt{2\pi}\pi^2)$ and $K(m)$ the complete elliptic

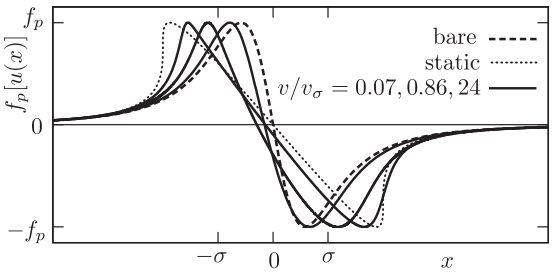

FIG. 8. Velocity dependence of the effective pinning force $f_p[u(x)]$ for a Lorentzian pin with Labusch parameter $\kappa = 1.0$ and for velocities $v/v_\sigma = 0.07, 0.86$, and 24. The dynamical force profile is compared to the bare force $f_p(x)$ (dashed) and the static effective force $f_p[u_s(x)]$ (dotted). The asymmetry in the effective pinning force $f_p[u(x)]$ (narrowing on the left as the vortex is dragged into the pin, broadening on the right as the vortex is held back in the pin) generates the finite pinning-force density $\langle F_p(v)\rangle$ at finite velocities, see Eq. (16).

integral of the first kind]

$$\langle F_p(v)\rangle \approx \nu^< \frac{n_p}{a_0\lambda\bar{C}}\sqrt{\frac{v}{v_\sigma}}\int_0^\infty dK\, K^4\sqrt{K\sigma}|e_p(K)|^2 \sim \frac{\sigma^2}{a_0\lambda}n_p\kappa f_p\sqrt{\frac{v}{v_\sigma}}, \tag{51}$$

where we provide a simple scaling estimate in the last line. Here, the velocity

$$v_\sigma = \sigma/t_{\rm th} \tag{52}$$

replaces v_p at weak pinning $\kappa < 1$. As expected, the average pinning force increases with velocity v from zero with a dependence $\propto\sqrt{v/v_\sigma}$; this result can be traced back to the time dependence $\propto t^{-3/2}$ of the 3D Green's function relevant at long times (and hence small velocities v) and a time integral that is cut on $t \sim 1/K_x v$.

The appearance of a finite pinning-force density for finite velocities v is illustrated in Fig. 8. In the static situation, the pinning-force density $\langle F_p(v=0)\rangle = F_c$ vanishes for the single-valued antisymmetric solution $u_s(x) = -u_s(-x)$ at weak pinning $\kappa \leqslant 1$. For finite velocities, the asymmetric deformation of the effective pinning force $f_p[u(x)]$ generates a finite positive result $\langle F_p(v)\rangle > 0$ instead.

The scaling $\propto\sqrt{v/v_\sigma}$ in the pinning-force density persists even beyond the Labusch point at $\kappa = 1$, the only relevant change being the appearance of a finite critical force density [6,17], $F_c \sim (\sigma x_s^f/a_0^2)n_p f_p(\kappa-1)^2$, see Eq. (42), while the velocity dependent part $[\langle F_p(v)\rangle - F_c] \propto\sqrt{v/v_\sigma}$ evolves smoothly across the Labusch point.

Next, we remain in the weak pinning regime and follow the evolution of the average pinning-force density $\langle F_p(v)\rangle$ with increasing velocity. We use the perturbative result for the average pinning-force density Eq. (47) in order to find a simple estimate for the evolution of $\langle F_p(v)\rangle$. The integration over space contributes a factor σ^2 due to the pin extension, the force derivative is estimated as $\partial_x f_p(x) \sim f_p/\sigma$, and the time integral over the Green's function contributes a factor $tG(0,t)$; the conversion from time to velocity again involves the pin size σ, $v \sim \sigma/t$. Starting from small velocities v, we choose the appropriate Green's function and obtain the results (with $\kappa < 1$)

$$\langle F_p(v)\rangle \sim \frac{\sigma^2}{a_0^2}n_p\kappa f_p\begin{cases}\frac{a_0}{\lambda}\sqrt{\frac{v}{v_\sigma}}, & \frac{v}{v_\sigma} < \frac{a_0^2}{\lambda^2},\\ \frac{v}{v_\sigma}, & \frac{a_0^2}{\lambda^2} < \frac{v}{v_\sigma} < 1,\\ \sqrt{\frac{v_\sigma}{v}}, & 1 < \frac{v}{v_\sigma},\end{cases} \tag{53}$$

with a maximal pinning force $\sim(\sigma/a_0)^2 n_p\kappa f_p$ appearing at v_σ. For weak pinning, all these results remain within the perturbative regime with $|\delta u| < \sigma$. This is no longer true if we turn to very strong pinning with $\kappa \gg 1$.

2. *Very strong pins $\kappa \gg 1$, large $v > \kappa v_p$*

For very strong pinning $\kappa \gg 1$, we have to make sure that the displacement u_p remains small, $u_p < \sigma$. A simple estimate of Eq. (46) provides the high-velocity result (we consider short times and hence use the 1D Green's function)

$$u_p(x) = \int_0^\infty dt G(0,t) f_p(x - vt) \sim \sigma\sqrt{\frac{\kappa v_p}{v}}. \tag{54}$$

Hence, for very strong pinning, perturbation theory becomes applicable only at very large velocities $v > \kappa v_p$.

In this high-velocity regime, we can make use of Eq. (51) and the 1D Green's function Eq. (22) to find an accurate expression for the mean pinning force density (with the numerical $\nu^> \approx 2[\Gamma(3/4)]^2/(\sqrt{2\pi}\pi^2)$)

$$\langle F_p(v)\rangle \approx \nu^> \frac{n_p}{a_0^2\bar{C}}\sqrt{\frac{v_\sigma}{v}}\int_0^\infty dK\,(K^4/\sqrt{K\sigma})|e_p(K)|^2 \sim \frac{\sigma^2}{a_0^2}n_p f_p\sqrt{\frac{\kappa v_p}{v}}. \tag{55}$$

The last estimate is consistent with a transverse trapping length $t_\perp \sim \sigma$, which is reduced by a factor $\kappa^{1/(n+2)}$ with respect to the static result of Eq. (33). As the velocity drops below κv_p, new effects show up which require a self-consistent evaluation of the vortex dynamics.

Before turning to this intermediate velocity regime, we comment on the relation between weak collective pinning theory and our single-pin approximation discussed above. Indeed, one can show (see Appendix B) that adopting the cutoff scheme of weak collective pinning to the strong pinning result Eq. (47), one can obtain a finite critical current density $j_c \propto n_p^2$, in agreement with the results obtained from weak collective pinning theory [17]. This finding is quite remarkable, as it provides an order n_p^2 result (that includes pin-pin correlations) from a standard $\propto n_p$ strong pinning approach by using an appropriate cutoff scheme.

C. Universal self-consistent dynamical solution for very strong pins with $\kappa \gg 1$

Upon decreasing the velocity v below κv_p in the very strong pinning regime, one has to account for the large deformation of the vortex before depinning. This is illustrated in Fig. 7, where the effective pinning force extends over a region $t_\parallel$ larger than σ and reaches $x_s^p \sim \kappa\sigma$ at sufficiently low velocities. Here, we attempt to use Eq. (15) to find a self-consistent solution for

the effective pinning force $f_p[u(x)]$ in the regime where the vortex deformation is still large.

In the very strong pinning regime and for velocities $v > v_p$ the largest time scale in the depinning process is given by $t \approx \kappa\sigma/v_p = t_{\rm th}$ and hence the relevant Green's function entering Eq. (15) is given by the 1D expression Eq. (22). The self-consistency equation (15) then can be written as

$$u(x) - x = \frac{1}{\bar{C}\sqrt{vt_{\rm th}}} \int_{-\infty}^{x} dx' \, \frac{f_p[u(x')]}{\sqrt{x - x'}}. \tag{56}$$

This equation can be solved in three regimes. (i) For $x < -\sigma$, the vortex does not yet feel the pin and the equation is trivially solved by $u(x) = x$. (ii) Similarly, for $x > t_\parallel$, the vortex has depinned and again $u(x) = x$. (iii) In the intermediate region $-\sigma < x < t_\parallel \leqslant \kappa\sigma$, we make use of the ansatz $f_p[u(x')] = -\alpha f_p \sqrt{x' + \sigma}$ [see also the discussion leading to Eq. (45) in Sec. IV A above] and find that

$$\begin{aligned} x - u(x) &= \frac{\alpha\, f_p}{\bar{C}\sqrt{vt_{\rm th}}} \int_{-\sigma}^{x} dx' \, \sqrt{(x' + \sigma)/(x - x')} \\ &= \frac{\alpha\, \pi\, f_p}{2\bar{C}\sqrt{vt_{\rm th}}} (x + \sigma). \end{aligned} \tag{57}$$

Dropping the small corrections $u(x) \lesssim \sigma \ll x$ on both sides of the equation, we find that the constant $\alpha = 2\bar{C}\sqrt{vt_{\rm th}}/\pi f_p \approx 2\sqrt{vt_{\rm th}}/\pi\kappa\sigma$ provides a consistent solution, resulting in the dynamical effective pinning force

$$f_p[u(x \gg \sigma)] \approx -\frac{2}{\pi}\bar{C}\sqrt{vt_{\rm th}x} \sim -f_p\sqrt{\frac{v}{v_p}\frac{x}{\kappa\sigma}}. \tag{58}$$

At depinning, the force assumes its maximal value $-f_p$ and we find the longitudinal trapping length

$$t_\parallel(v > v_p) \approx \frac{\pi^2}{4}\left(\frac{f_p}{\bar{C}}\right)^2 \frac{1}{vt_{\rm th}} \sim \frac{v_p}{v}\kappa\sigma, \tag{59}$$

starting from σ at high velocities $v \sim \kappa v_p$ and increasing to the maximal value $t_\parallel(v_p) \sim \kappa\sigma$ as v drops to v_p, see Sec. III. One easily checks that we indeed remain in the 1D elastic regime throughout this range of velocities: for velocities v larger than v_p one finds that the relevant time $t \sim t_\parallel(v)/v \sim t_{\rm th}$ $(v_p/v)^2 < t_{\rm th}$.

Combining Eqs. (58) and (59), we can provide a good approximation for the behavior of the dynamical effective pinning force at large values of $x \gg \sigma$,

$$f_p[u(x \gg \sigma)] \approx -f_p\sqrt{x/t_\parallel(v)}. \tag{60}$$

When the vortex depins at $t_\parallel(v)$, it attains its original straight shape back within a thermal time $t_{\rm th}$; this follows from the dissipative equation of motion for a vortex segment a_0 that is displaced by u, $\eta_l a_0 u/t_{\rm dp} \sim \varepsilon_0 u/a_0$ (with $\eta_l = \eta a_0^2$ the line friction), from which we obtain $t_{\rm dp} \sim \eta a_0^4/\varepsilon_0 \sim t_{\rm th}$, see Eq. (19). During this depinning process, the vortex moves by a distance $x_{\rm dp} \sim vt_{\rm th} = \sigma v/v_\sigma$. As v increases beyond v_σ, the depinning process smoothens, the depinning time is determined by the average motion, $t_{\rm dp} \sim \sigma/v$, and the depinning distance $x_{\rm dp}$ saturates at σ,

$$x_{\rm dp}(v) \sim \begin{cases} \sigma v/v_\sigma, & v < v_\sigma, \\ \sigma, & v_\sigma < v. \end{cases} \tag{61}$$

These results describe qualitatively well the depinning curves in Fig. 7.

Making use of the dynamical effective pinning force (58) in the expression for the average pinning force (14) and cutting the integral on $t_\parallel(v)$, we find that $\langle f_p(v)\rangle$ decays $\propto v_p/v$ over the extended velocity regime $v_p < v < \kappa v_p$,

$$\langle f_p(v)\rangle \approx \frac{\pi^2}{6} f_p \left(\frac{f_p}{\bar{C}a_0}\right)^2 \frac{a_0}{vt_{\rm th}} \sim \frac{\kappa\sigma}{a_0}\frac{v_p}{v} f_p, \tag{62}$$

where we have replaced $f_p/\bar{C}\sigma \approx \kappa$ in the second expression. The pinning-force density $\langle F_p(v)\rangle$ requires knowledge of the transverse pinning or trapping length $t_\perp(v)$ which will be calculated in Sec. IV E.

D. Perturbation theory around static solution

At low velocities, the dynamical force $f_p[u(x)]$ remains close to the static one $f_p[u_s(x)]$, as illustrated in the example of a Lorentzian potential shown in Fig. 7. The basic idea then is to construct a perturbative analysis away from the static solution $u_s(x)$; the latter rests on a reformulation of the dynamical equation (15) that makes use of the integrated Green's function

$$G^\uparrow(x) = \int_x^\infty \frac{dx'}{v} G(0, x'/v) \tag{63}$$

and rewriting the Green's function $G[(x - x')/v]$ in Eq. (15) through the derivative $-v\partial_x G^\uparrow(x - x')$. Interchanging the derivative and the integral, we can extract a term $f_p[u(x)]/\bar{C}$ and arrive at a formula reminiscent of the static variant (23),

$$u(x) = [x - \delta x[u](x)] + \frac{f_p[u(x)]}{\bar{C}}, \tag{64}$$

with the coordinate shift

$$\delta x[u](x) = \partial_x \int_{-\infty}^{x} dx' G^\uparrow(x - x') f_p[u(x')]. \tag{65}$$

The dynamic solution $u(x)$ then can be expressed [14] through the smooth multivalued static solution $\bar{u}_s(x)$ via the self-consistent coordinate shift $\delta x[u](x)$,

$$u(x) = \bar{u}_s[x - \delta x[u](x)] \equiv \bar{u}_s[x_{\rm eff}[u](x)]. \tag{66}$$

Here, the smooth static solution $\bar{u}_s(x)$ follows the free, unstable, and pinned branches and thus differs from $u_s(x)$ by a substitution of the jumps by the unstable branches. One easily checks that evaluating the static self-consistency equation (23) at $x - \delta x$ and making use of Eq. (66) reproduces the dynamical equation (64).

The integrated Green's function (63) relevant in the coordinate shift $\delta x[u](x)$ assumes the form

$$G^\uparrow(x) \approx \begin{cases} \frac{1}{\bar{C}}, & \frac{x}{vt_{\rm th}} < 1, \\ \frac{1}{2\sqrt{2\bar{C}}}\frac{vt_{\rm th}}{x}, & 1 < \frac{x}{vt_{\rm th}} < \frac{\lambda^2}{a_0^2}, \\ \frac{1}{\sqrt{2}\pi}\frac{a_0}{\lambda}\frac{1}{\bar{C}}\sqrt{\frac{vt_{\rm th}}{x}}, & \frac{\lambda^2}{a_0^2} < \frac{x}{vt_{\rm th}}. \end{cases} \tag{67}$$

In the static limit $v \to 0$, the coordinate shift $\delta x[u](x) = 0$ vanishes, except for two finite spikes of vanishing width $\propto \sqrt{v}$ at $-x_s^f$ and x_s^p, and the dynamic displacement approaches the static one, $u(x) \to u_s(x)$. Substantial changes in $\delta x[u](x)$ (and hence in $u(x)$ and $\langle f_p(v)\rangle$) are to be expected when the

scale $vt_{\rm th}$ of $G^{\uparrow}(x)$ increases beyond the pinning scale $\kappa\sigma$ of $f_p[u(x)]$, confirming the estimate $v_p \sim \kappa\sigma/t_{\rm th}$ for the pinning velocity scale in Eq. (43).

Given the shape of the displacement $\bar{u}_s(x)$ as discussed above and illustrated in Fig. 3(a), let us first understand how this static solution generates the dynamic solution $u(x)$ via the coordinate shift $\delta x[u](x)$, see (66)—the precise understanding of this mapping is an important step in the construction of the perturbative analysis of the dynamical displacement $u(x)$ at small velocities v discussed below. The most noticeable feature in the static solution $u_s(x)$ are the jumps at $-x_s^f$ and x_s^p marking the trapping of the vortex tip and its depinning. These jumps imply that the vortex does not probe all of the pin potential. In the dynamic situation, the vortex tip moves with a finite velocity across the pin and thus has to pass every point in the pinning potential at some time, hence the dynamical solution $u(x)$ has to be continuous in x. The relation (66) maps the continuous function $u(x)$ via the shift function $\delta x[u](x)$ to the static solution $\bar{u}_s(x)$ of Eq. (23), where $u(x)$ probes all three branches of the static solution $\bar{u}_s(x)$, free, unstable, and pinned ones. In order to do so, the shift $\delta x[u](x)$ or the effective coordinate $x_{\rm eff}[u](x) = x - \delta x[u](x)$ has to develop (sharp) negative spikes close to the points $-x_s^f$ and x_s^p, see Fig. 3(b). These spikes start at the shifted positions $-x^f$ and x^p defined through the conditions [see Eq. (66) and note that $u(-x^f) = u_s(-x_s^f)$ and $u(x^p) = u_s(x_s^p)$, see Figs. 3(a) and 3(b)]

$$-x^f - \delta x[u](-x^f) = x_{\rm eff}[u](-x^f) = -x_s^f, \tag{68}$$

$$x^p - \delta x[u](x^p) = x_{\rm eff}[u](x^p) = x_s^p. \tag{69}$$

The height of these spikes are such as to shift the unstable branches $u_s^u(x)$ to the dynamical solution $u(x)$ [dotted arrows in Fig. 3(a)]. It turns out, that the shift function $\delta x[u](x)$ is the central quantity in the perturbative calculation of $\langle f_p(v)\rangle$.

Our goal then is to find the correction in the average pinning force

$$\langle f_p(v)\rangle - f_c \equiv \langle \delta f_p(v)\rangle = -\frac{1}{a_0}\int_{-\infty}^{\infty} dx\,(f_p[u(x)] - f_p[u_s(x)]). \tag{70}$$

The difficulties with the evaluation of Eq. (70) are the steep slopes in $u(x)$ and jumps in $u_s(x)$ when the vortex enters and leaves the pin, see Fig. 3. While the jumps in $u_s(x)$ appear at the positions $-x_s^f$ and x_s^p, these positions are shifted to $-x^f$ and x^p for the dynamical solution $u(x)$. At the locations $-x_s^f$, $-x^f$, x^p, and x_s^p either the static ($f_p[u_s(x)]$) or dynamic ($f_p[u(x)]$) force changes rapidly between free and pinned branches. We then can split the integral in Eq. (70) into appropriate intervals with and without jumps,

$$\langle \delta f_p(v)\rangle = -\frac{1}{a_0}\left[\int_{-\infty}^{-x_s^f} dx\,\delta f_{ff}(x) + \int_{-x_s^f}^{-x^f} dx\,\delta f_{fp}(x) + \int_{-x^f}^{x^p} dx\,\delta f_{pp}(x) + \int_{x^p}^{x_s^p} dx\,\delta f_{fp}(x) + \int_{x_s^p}^{\infty} dx\,\delta f_{ff}(x)\right], \tag{71}$$

where

$$\delta f_{ab}(x) \equiv f_p\big[u_s^a(x - \delta x[u](x))\big] - f_p\big[u_s^b(x)\big] \tag{72}$$

and u_s^a with $a \in \{f, p\}$ denote free and pinned branches of the static solution $u_s(x)$ (we have expressed $u(x)$ through Eq. (66) but do not resolve the steep rise in $u(x)$ on the unstable branch). The contributions of the various terms in Eq. (71) to the average pinning force is given in Appendix C. It turns out that only the third and the fourth term are relevant; furthermore, their contribution can be expressed in a closed form that contains only the static solution $u_s(x)$,

$$\langle \delta f_p(v)\rangle \approx \frac{1}{a_0}\left(\int_{-x_s^f}^{x_s^p} dx\,\partial_x f_p\big[u_s^p(x)\big]\,\delta x\big[u_s^p\big](x) + \delta x\big[u_s^p\big]\big(x_s^p\big)\left\{f_p\big[u_s^f\big(x_s^p\big)\big] - f_p\big[u_s^p\big(x_s^p\big)\big]\right\}\right). \tag{73}$$

An equivalent formula was obtained by Larkin and Ovchinnikov in Ref. [14] for a periodic pinning model describing large defects; the regularization introduced in their analysis follows from our derivation.

1. *Very strong pinning with $\kappa \gg 1$*

Making use of the universal solution for the static strong pinning force in Sec. III C, we can find the sign of the small-velocity behavior of $\langle \delta f_p(v)\rangle$. We replace the force gradient by the (negative) effective elasticity $-\bar{C} \approx -f_p/\kappa\sigma$ in the first term and set the forces to zero and to $-f_p$ on the free and pinned branches in the second term to arrive at

$$\langle \delta f_p(v)\rangle \approx -\frac{f_p}{a_0}\left[\int_{-x_s^f}^{x_s^p} dx\,\frac{\delta x\big[u_s^p\big](x)}{\kappa\sigma} - \delta x\big[u_s^p\big]\big(x_s^p\big)\right] = -\frac{f_p}{a_0}\big[\overline{\delta x\big[u_s^p\big](x)} - \delta x\big[u_s^p\big]\big(x_s^p\big)\big], \tag{74}$$

where $\overline{\cdots}$ denotes the average over the interval $[-x_s^f, x_s^p]$. Finally, we use again the linear form $-\bar{C}x$ for the effective pinning force and the expression (67), $G^{\uparrow} \propto 1/\sqrt{x}$ (valid in the limit $v \to 0$) for the integrated Green's function, in the calculation of the coordinate shift $\delta x[u_s^p](x)$,

$$\delta x\big[u_s^p\big](x) \approx -\bar{C}\partial_x \int_0^x dx' G^{\uparrow}(x - x')\,x' \sim -\sigma\frac{a_0}{\lambda}\sqrt{\frac{v\,x}{v_\sigma\,\sigma}}. \tag{75}$$

Here, we have ignored the part of δx describing the jump into the pin by starting the integration from $x = 0$. Making use of Eq. (75) in (74), the dynamical pinning force correction then assumes a negative value,

$$\langle \delta f_p(v)\rangle \sim -\frac{a_0}{\lambda} f_c \sqrt{\frac{v}{v_p}}. \tag{76}$$

This negative correction can be easily understood by noting that $-\delta x[u_s^p](x)$ is a monotonically increasing positive function and hence the second (boundary) term in (74) always dominates over the average in the first term.

The above result applies to the very strong pinning situation with $\kappa \gg 1$. On the other hand, we have seen in Sec. IV B 1 that the pinning-force density is positive, $\langle F_p(v)\rangle \propto \sqrt{v/v_\sigma}$ when pinning is weak and $F_c = 0$. The question arises about the origin of the sign change in $\langle \delta f_p(v)\rangle$ and for which value of κ this sign change occurs.

2. *Moderately strong pinning with $\kappa \gtrsim 1$*

In order to understand the sign change in $\langle \delta f_p(v)\rangle$, we have to be more accurate in our description of $f_p[u_s^p(x)]$ near depinning at x_s^p, as it is the last term in Eq. (74) that is strongly modified when κ decreases, while the first term remains unchanged. Indeed, as κ decreases, the decrease $f_p/2\kappa^2$ in the magnitude of $f_p[u_s^p(x)]$ before the jump at x_s^p increases, see Eq. (A3), leaving a smaller jump at x_s^p. Furthermore, the coordinate shift $\delta x[u_s^p](x)$ starts decreasing before the jump such that $x_s^p - x^p$ becomes small. These modifications lead to a reduction of the second term in Eq. (74), which is nothing but the signature of a decreasing critical force average f_c.

More precisely, we can use the result Eq. (A3) for the static pinning force $f_p[u_s(x)] = f_p[u_s^p(x)]$ to obtain a more accurate expression for the coordinate shift. We make use of the expression (67) for the integrated Green's function, $G^\uparrow(x - x') \propto \sqrt{vt_{\rm th}/(x-x')}$ for $x - x' > vt_{\rm th}$, cut the integral at $x' = x - vt_{\rm th}$, and concentrate on the leading terms which are large close to $x \approx x_s^p$ to obtain

$$\begin{aligned}\delta x[u](x) \approx \delta x\big[u_s^p\big](x) &\approx \frac{\partial}{\partial x}\int_{-\infty}^{x} dx' G^\uparrow(x-x')\, f_p\big[u_s^p(x')\big] \\ &\approx -\frac{\sqrt{2}\sigma}{\pi}\frac{a_0}{\lambda}\sqrt{\frac{v}{v_\sigma}} \\ &\quad\times\left(\sqrt{\frac{x}{\sigma}} - \sqrt{\frac{\sigma\bar{C}}{8f_p}}\ln\frac{\sqrt{x_s^p}+\sqrt{x}}{\sqrt{x_s^p}-\sqrt{x-vt_{\rm th}}}\right). \qquad (77)\end{aligned}$$

As expected, the coordinate shift is small in $\sqrt{v}$ and increases in magnitude $\propto\sqrt{x}$, see Eq. (75). However, due to the decrease in the magnitude of the pinning force on approaching x_s^p, a logarithmic correction appears, leading to a sharp collapse of δx at x_s^p, which is cutoff (due to the transition to the single-vortex response) by the term $vt_{\rm th}$. Inserting the result (77) into the expression (74), we find that the velocity correction to the average pinning force assumes the form

$$\begin{aligned}\langle \delta f_p(v)\rangle &\approx \frac{\sqrt{2}\big(x_s^p + x_s^f\big)}{3\pi\lambda} f_p\sqrt{\frac{vt_{\rm th}}{x_s^p + x_s^f}} \\ &\quad\times\left(-1 + \frac{3}{8\sqrt{2}}\frac{\sigma\bar{C}}{f_p}\ln\frac{4v_p}{v}\right) \\ &\sim \frac{\kappa\sigma}{\lambda} f_p\sqrt{\frac{v}{v_p}}\left(-1 + \frac{3}{8\sqrt{2}}\frac{\sigma\bar{C}}{f_p}\ln\frac{4v_p}{v}\right). \qquad (78)\end{aligned}$$

This more accurate analysis shows that $\langle \delta f_p(v)\rangle$ always increases with v at very small velocities v, however, the corresponding velocity range is exponentially small in $\kappa \sim f_p/\sigma\bar{C}$, $v < v_p\exp(-\nu\kappa)$ with $\nu = (2\sqrt{2}/3)\,4 \approx 4$, and therefore irrelevant at very strong pinning with $\kappa \gg 1$. Indeed, the small upturn predicted by Eq. (78) is not visible in Fig. 6. The result Eq. (78) straightforwardly provides the pinning-force density $\langle F_p(v)\rangle$ when combined with the result for the transverse trapping length $t_\perp(v)$ derived in the next section.

E. Dynamical transverse trapping length $t_\perp$

The transverse trapping length $t_\perp$ has been found for the two limits of static pinning at vanishing velocity $v = 0$ and in the perturbative high-velocity regime $v > \kappa v_p$. The static limit has been discussed in Sec. III B, providing us with the result $t_\perp = R_s^f$, the asymptotic position where the free-branch minimum of the total pinning energy $e_t(R;r)$ in Eq. (31) vanishes; for a very strong pin with tails, $R_s^f \sim \sigma\kappa^{1/(n+2)}$. This result is parametrically larger than the one we found at very large velocities $v > \kappa v_p$ using perturbation theory where $t_\perp \sim \sigma$, see Sec. IV B 2. The question then poses itself, how the transverse trapping length shrinks from $t_\perp \sim \sigma\kappa^{1/(n+2)}$ to $t_\perp \sim \sigma$ as the velocity v increases.

We start from the static situation and consider the spherically symmetric total energy of Eq. (31) at the critical radius R_s^f where the first and second derivatives vanish, $\partial_r e_t(R;r)|_{R_s^f,r_s^f} = 0$ and $\partial_r^2 e_t(R;r)|_{R_s^f,r_s^f} = 0$, and the free branch disappears. We consider the limit of very strong pinning (otherwise $t_\perp \sim \sigma$ follows trivially) and assume a pinning potential with long tails, $e_p(r) \sim -e_p\,(\sigma/r)^n$, $n = 2$ for a Lorentzian-shape defect potential. The critical asymptotic (R_s^f) and tip ($r_s^f < R_s^f$) positions where the free branch terminates then can be estimated to be located at the radii $R_s^f \gtrsim r_s^f \sim \sigma\kappa^{1/(n+2)}$, where we have dropped numericals and set $\kappa \sim e_p/\sigma^2\bar{C}$. The expansion of the total potential at R_s^f in the vicinity of r_s^f then is given by the cubic parabola [we drop a constant of order $\bar{C}\,(r_s^f)^2$]

$$e_t\big(R_s^f;r\big) = \frac{\alpha}{3}\big(r - r_s^f\big)^3, \quad \alpha \sim \frac{\bar{C}}{r_s^f}. \qquad (79)$$

The vortex tip (in the form of a segment of length a_0) then follows the equation of motion $\eta_l a_0\,\dot{r} = -\partial_r e_t = -\alpha(r - r_s^f)^2$; in the static limit, every vortex approaching the defect with an impact parameter $b < R_s^f$ will fall to the center, having an infinity of time available to overcome the flat potential around r_s^f. In the dynamical situation, the vortex passes the pin with a finite velocity v and we have to include an additional force-term $-\bar{C}[R_s^f - R(t)]$ in the equation of motion; here, $\mathbf{R}(t) = (-X^f + vt, Y^f)$ denotes the moving asymptotic position of the vortex entering the critical radius R_s^f around the defect at $t = 0$ from the left. Assuming an impact parameter b close to R_s^f, we can expand $R(t) \approx R_s^f(1 - X_s^f vt/(R_s^f)^2)$, where we follow the trajectory over a time $t \leqslant X_s^f/v \equiv t_{\rm tra}$ to $X = 0$, half the time to traverse the defect potential. The equation of motion

$$\eta_l a_0\,\dot{r} = -\alpha\big(r - r_s^f\big)^2 - \bar{C}\big(X_s^f/R_s^f\big)vt \qquad (80)$$

then picks up an additional force-term that is linear in time t and independent on position r. Therefore, Eq. (80) can be brought to the form of Riccati's equation [37], $\dot{\bar{r}} = \bar{r}^2 + \bar{t}$, where we have introduced the dimensionless variables $\bar{r}$ and $\bar{t}$ via $r = r_s^f(1 - \beta^{1/3}\bar{r})$ and $t = t_{\rm th}\beta^{-1/3}\bar{t}$ with $\beta = (X_s^f/R_s^f)\,vt_{\rm th}/r_s^f$. Starting from $\bar{r}(\bar{t} = 0) = 0$, the radius $\bar{r}$

starts out small and we can drop the $\bar{r}^2$ term to find the solution $\bar{r}(\bar{t}\,) \approx \bar{t}^{\,2}/2$. When $\bar{r}$ is large, we can drop the $\bar{t}$ term and obtain the solution $\bar{r}(\bar{t}\,) \approx 1/(\bar{t}^* - \bar{t})$ with $\bar{t}^*$ an integration constant of order unity. In order to find the precise location of the divergence, one has to perform a numerical integration that provides the result $\bar{t}^* \approx 1.986$, see Ref. [37]. Thus we find that the vortex tip falls to the center within the time window (we use $\bar{t}^* \approx 2$)

$$t_{\rm fall} \lesssim 2t_{\rm th}\left(\frac{r_s^f R_s^f}{X_s^f\, v t_{\rm th}}\right)^{1/3}. \tag{81}$$

The vortex tip has to fall to the center within a time smaller than $t_{\rm tra} \approx X_s^f/v$, from which we find the condition $(X_s^f)^2 \gtrsim R_s^f\, v t_{\rm th}$ (we approximate $r_s^f \approx R_s^f$). We thus obtain an upper limit on the impact parameter $b = [(R_s^f)^2 - (X_s^f)^2]^{1/2}$ of vortices that can be trapped, what provides us with a result for the transverse trapping length $t_\perp(v)$ at small velocities,

$$R_s^f - t_\perp(v) \sim \frac{v t_{\rm th}}{R_s^f}. \tag{82}$$

The above analysis applies to impact parameters b close to R_s^f (or small X_s^f) where the tip trajectory is dominated by the slow motion near r_s^f. At small impact parameters b of order a fraction of R_s^f, the elastic term in e_t is no longer relevant and we have to consider the motion of the vortex tip in the radial pinning potential $e_p(r)$. The equation of motion then has to be replaced by $\eta_l a_0 \dot{r} \sim -f_p(\sigma/r)^{n+1}$ and its integration leads to the trajectory

$$r(t) = r_0(1 - t/t_{\rm fall})^{1/(n+2)}, \quad t_{\rm fall} \sim t_{\rm th}\left(\frac{r_0}{R_s^f}\right)^{n+2}, \tag{83}$$

where r_0 denotes the starting radius at $t = 0$. The fastest fall to the center appears at the closest approach to the defect and hence we choose $r_0 \sim b$. Again, the time to fall to the center has to be smaller than the traversing time which we estimate as $t_{\rm tra} \sim b/v$ as given by the geometry of the problem. We thus find that trajectories with an impact parameter

$$b < t_\perp(v) \sim R_s^f\left(\frac{R_s^f}{v t_{\rm th}}\right)^{1/(n+1)} \tag{84}$$

fall into the pin. The above result applies for velocities such that $t_\perp \gtrsim \sigma$, i.e., for $v > v_p$.

Combining the results (82) and (84), we find that the trapping length $t_\perp(v)$ decreases with increasing velocity v on the velocity scale $R_s^f/t_{\rm th} \sim v_p/\kappa^{(n+1)/(n+2)}$, first with a correction factor $\propto 1 - \kappa^{(n+1)/(n+2)} v/v_p$ and then with a power law $\propto [v_p/(\kappa^{(n+1)/(n+2)} v)]^{1/(n+1)}$. Hence the transverse length $t_\perp(v)$ decreases from R_s^f at $v = 0$ to σ at a velocity v_p.

The two trapping lengths $t_\perp(v)$ and $t_\parallel(v)$, see Eq. (59), define the trapping area $S_{\rm trap}(v) = 2t_\perp(v)t_\parallel(v)$ which decreases smoothly from $S_{\rm trap} \sim \kappa^{(n+3)/(n+2)}\sigma^2$ at $v = 0$ to $S_{\rm trap} \sim \sigma^2$ at $v \sim \kappa v_p$ and remains constant thereafter. Within the region $0 < v < v_p$, this decrease is due to the reduction of $t_\perp$ from $\kappa^{1/(n+2)}\sigma$ to σ, while for velocities $v_p < v < \kappa v_p$ it is the longitudinal length $t_\parallel$ that shrinks from $\kappa\sigma$ to σ.

We note that the velocity scale $v_\sigma \kappa^{1/(n+2)}$ can also been obtained from a perturbative analysis: for a vortex with asymptotic position $-x < 0$ passing the pin's center at $t = 0$, the pinning-induced correction (46) can be estimated as

$$u_p \sim \frac{\kappa\sigma^{n+2}}{t_{\rm th}}\left[\int_0^{t_{\rm th}} dt\left(\frac{t_{\rm th}}{t}\right)^{1/2} + \int_{t_{\rm th}}^{\infty} dt\left(\frac{t_{\rm th}}{t}\right)^{3/2}\right] \times \frac{x + vt}{[\sigma^2 + (x + vt)^2]^{(n+2)/2}}. \tag{85}$$

For small velocities $v < x/t_{\rm th}$, the integral assumes its main contribution from $t \sim t_{\rm th}$ and we find that $u_p \sim \kappa\sigma\,(\sigma/x)^{n+1}$, while for larger velocities the integral is cut at v/x and $u_p \sim \kappa\sigma\,(\sigma/x)^{n+1}(x/v t_{\rm th})^{1/2}$. The perturbation theory breaks down when $u_p \sim x$, i.e., at the distance x_s^f at small velocities and at $x_s^f\,(v_\sigma\kappa^{1/(n+2)}/v)^{1/2(n+3/2)}$ at high velocities, implying a reduction of the large-distance perturbative region on the velocity scale $v_\sigma\kappa^{1/(n+2)}$.

F. Summary of force densities

We conclude this section with a summary of results for the dynamic pinning force density $\langle F_p(v)\rangle (= F_c + \langle \delta F_p(v)\rangle)$ on the level of dimensional estimates. For small and intermediate velocities $v < \kappa v_p$, more accurate expressions are obtained by combining the results for the average pinning force $\langle f_p(v)\rangle$, Eqs. (30), (62), and (78), with those for the transverse trapping length $t_\perp(v)$, Eqs. (82) and (84), and using Eq. (16). At high velocities $v > \kappa v_p$, the perturbative result Eq. (55) for $\langle F_p(v)\rangle$ can be used.

Starting out at $v = 0$, we have the critical force density

$$F_c \sim \frac{\kappa\sigma x_s^f}{a_0^2} n_p f_p \frac{(\kappa - 1)^2}{\kappa^2} \tag{86}$$

in a form that is valid for all values $\kappa \geqslant 1$. The corrections at small velocities $v < v_p$ are given by $\langle \delta F_p(v)\rangle = (2t_\perp(v)/a_0) n_p \langle \delta f_p(v)\rangle$ with

$$\langle \delta f_p(v)\rangle \sim \begin{cases} -\frac{\kappa\sigma}{\lambda} f_p \left(\frac{v}{v_p}\right)^{\frac{1}{2}}, & \frac{v}{v_p} < \frac{a_0^2}{\lambda^2}, \\ -\frac{\kappa\sigma}{a_0} f_p \frac{v}{v_p}, & \frac{a_0^2}{\lambda^2} < \frac{v}{v_p} < 1, \end{cases} \tag{87}$$

and

$$t_\perp(v) \sim \begin{cases} x_s^f\left(1 - \frac{v\kappa^{\frac{n+1}{n+2}}}{v_p}\right), & \frac{v}{v_p} \ll \kappa^{-\frac{n+1}{n+2}}, \\ x_s^f\left(\frac{v_p}{v\kappa^{\frac{n+1}{n+2}}}\right)^{\frac{1}{n+1}}, & \kappa^{-\frac{n+1}{n+2}} < \frac{v}{v_p} < 1, \\ \sigma, & 1 < \frac{v}{v_p}. \end{cases} \tag{88}$$

The corresponding results for moderate values of κ remain unchanged up to a sign change in $\langle \delta f_p(v)\rangle$, i.e., $\langle f_p(v)\rangle$ increases with v. Increasing the velocity beyond v_p, we have the following results for the pinning-force density $\langle F_p(v)\rangle$, see Eqs. (62) and (55),

$$\langle F_p(v)\rangle \sim \frac{\kappa\sigma^2}{a_0^2} n_p f_p \begin{cases} \frac{v_p}{v}, & 1 < \frac{v}{v_p} < \kappa, \\ \sqrt{\frac{v_p}{\kappa v}}, & \kappa < \frac{v}{v_p}. \end{cases} \tag{89}$$

Again, these results remain valid as κ is reduced towards the Labusch point. Note that all of the above results smoothly join at the respective boundaries.

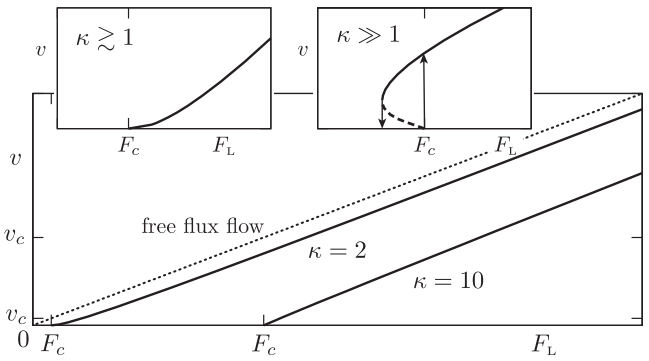

FIG. 9. Illustration of the force-velocity curve in the dilute limit for $n_p a_0 \sigma^2 \kappa = 0.05$. In the absence of pinning, the velocity is given by $v = F_L/\eta$ (dotted line). In the presence of pinning, this line is shifted to $F_c \propto n_p$ (solid line) and closely follows a shifted straight line of equal slope for velocities $v \ll v_p$. Corrections to this linear excess-force characteristic appear at velocities beyond v_p, which does not depend on the small pin density n_p, or at small velocities $\propto n_p^2$ (see insets, the arrows refer to the hysteretic switching). Original figure published in Ref. [29].

V. FORCE-VELOCITY CHARACTERISTIC AT STRONG PINNING

We are now ready to find the force-velocity or current-voltage characteristic of the strong pinning superconductor in the dilute pin regime. The final task is to solve the dynamical equation (1), which we have already written in the convenient form Eq. (2). The analysis of Sec. IV has provided us with the velocity scale v_p for the average pinning-force density $\langle F_p(v)\rangle$. In the limit of small pin densities n_p, we find that the dissipative motion of the bulk vortex system involves the velocity $v_c = F_c/\eta$, which is much smaller than the typical depinning velocity v_p characteristic of the strong pinning physics; interpolating the results (40) and (42) for the critical force F_c, we find that the ratio

$$\frac{v_c}{v_p} \sim n_p a_0 \sigma^2 \frac{(\kappa-1)^2}{\kappa} \ll 1 \tag{90}$$

in the small pin-density limit at fixed $\kappa > 1$ [38]. The pinning-force density $\langle F_p(v)\rangle$ then remains essentially unchanged, $\langle F_p(v)\rangle \approx F_c$ for a large region of velocities including v_c and limited only by $v_p \gg v_c$. Hence the characteristic takes the generic form of a shifted (by F_c) linear (flux-flow) curve,

$$v \approx (F_L - F_c)/\eta, \quad v \ll v_p, \tag{91}$$

see Fig. 9. The free dissipative flow

$$v \approx F_L/\eta, \quad v_p \ll v, \tag{92}$$

is approached only at very high velocities $v \gg v_p \gg v_c$.

The simple excess-force characteristic is a consequence of the separation of velocity scales v_c and v_p; the latter merge at strong pinning with increasing density n_p when strong 3D pinning goes over into 1D strong pinning at [17] $n_p a_0 \sigma^2 \kappa \sim 1$. Using qualitative arguments, a similar excess-force characteristic has been found in Ref. [12].

The roughly constant behavior of the pinning-force density $\langle F_p(v)\rangle \approx F_c$ over a large velocity region $v < v_p$ is the analog to Coulomb's law of dry friction for the problem of strong vortex pinning. Hence although we have invested a large effort in the calculation of the velocity dependence of the pinning-force density $\langle F_p(v)\rangle$, the most important statement is that about the largeness of the scale v_p in comparison to v_c. The detailed dependence of $\langle F_p(v)\rangle$ on v in Eqs. (87) and (89) only manifests itself very close to and far away from F_c, e.g., when investigating the approach to the free flux flow at large drives $F_L \gg F_c$.

Besides the corrections at high velocities $v > v_p$ due to the velocity dependence of $\langle f_p(v)\rangle$, additional changes show up close to F_c and at very low velocities due to the square-root dependence $\langle F_p(v)\rangle - F_c \propto \pm\sqrt{v/v_p}$. The force balance equation then can be written in the form

$$\frac{F_L}{F_c} - 1 = \frac{v}{v_c} \pm \sqrt{\frac{v}{v_p^{\pm}}}, \tag{93}$$

with the small-velocity pinning scales $v_p^{\pm}$ deriving from Eq. (87),

$$v_p^- \sim \frac{\lambda^2}{a_0^2} v_p, \quad \kappa \gg 1, \tag{94}$$

$$v_p^+ \sim \frac{\lambda^2}{a_0^2} (\kappa-1)^4 v_p, \quad \kappa \to 1. \tag{95}$$

For strong pinning $\kappa \gg 1$, the negative (nonlinear) correction in the average pinning-force density generates a bistability (and hence hysteretic jumps [14]) on the scale $v_{nl} = v_c^2/v_p^- \propto n_p^2$. The unstable branch increases below F_c, according to $v \approx v_p^-(1 - F_L/F_c)^2$, turns around reaching a finite value $v = v_{nl}$ at $F_L = F_c$, and approaches the linear excess characteristic $v \approx v_c(F_L/F_c - 1) > v_{nl}$ for $F_L > F_c$. On the other hand, approaching the Labusch point $\kappa \to 1$, the correction changes sign and the velocity increases quadratically,

$$v \sim v_p^+ (F_L/F_c - 1)^2 < v_c^2/v_p^+ = v_{nl}, \tag{96}$$

reaches the value v_{nl} at $F_L/F_c = 1 + 2v_c/v_p^+$, and crosses over to the linear regime $v \approx v_c(F_L/F_c - 1) > v_{nl}$ at larger drive $F_L > F_c$. While these features are illustrated in the insets of Fig. 9 (showing an expanded view of the characteristic near onset), we have to caution the reader that these results, residing in the regime $v_{nl} \propto n_p^2$, may get modified due to collective pinning effects.

VI. MODEL PINS

In our discussion above, we have frequently made use of the Lorentzian-shaped pinning potential Eq. (4) in order to gain insights into the strong-pinning features of the dynamical vortex response. This specific example of a pinning potential is quite appropriate when performing a numerical analysis but is less convenient for analytical studies. The latter can be easily attacked for a bare pinning force $f_p(x)$ of polynomial form, at least in the static limit where we have to solve the self-consistency equation (23). It turns out, that for a linear-force profile, the analytic solution can be pushed further to finite velocities, motivating our study of pins with a truncated quadratic (or parabolic) pinning potential, see Fig. 10. However, the quadratic-potential pin formally describes a very

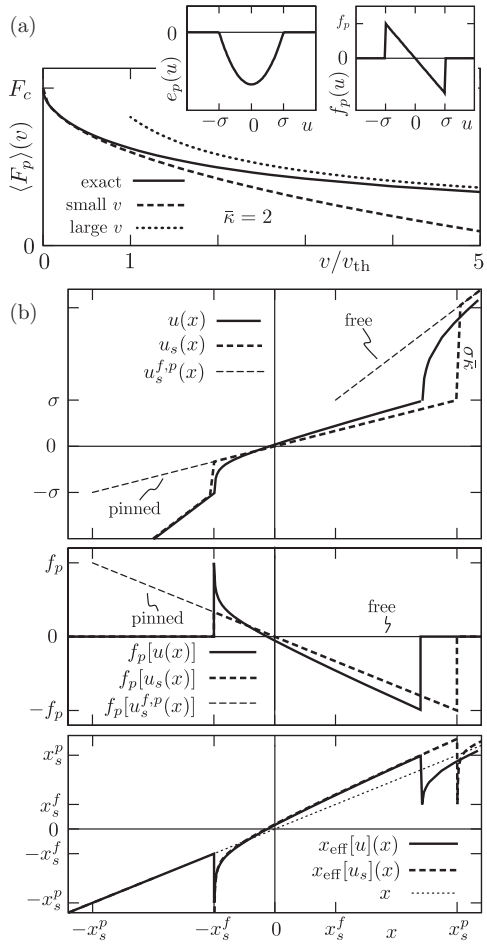

FIG. 10. (a) Pinning-force density vs velocity for a linear-force pinning model with strength $\bar{\kappa} = 2$ [the insets show a sketch of the bare pinning potential $e_p(x)$ and bare force $f_p(x)$]. The exact result (solid) is plotted for comparison with the results from the low- (dashed) and high-velocity (dotted) expansions. (b) Top to bottom: displacement field $u(x)$, force $f_p[u(x)]$, and effective coordinate $x_{\rm eff}[u](x)$ for a small velocity $v/v_p = 0.05$. The exact displacement field $u(x)$ and force $f_p[u(x)]$ (solid lines) are compared to the static quantities $u_s(x)$ and $f_p[u_s(x)]$ (dashed) for vortex motion from left to right. Also shown are the free $[u_s^f(x)$ and $f_p[u_s^f(x)]$, light dashed] and pinned branches $[u_s^p(x)$ and $f_p[u_s^p(x)]$, light dashed], with the multivalued static solution within the interval $x_s^f < |x| < x_s^p$. The exact effective coordinate $x_{\rm eff}[u](x)$ (solid line) is compared to the approximation $x_{\rm eff}[u_s](x)$ (dashed).

strong pin with a Labusch parameter $\kappa \to \infty$, since the force jumps to zero at the pin's edges at $x = \pm\sigma$. In order to study pinning at intermediate values of κ and the approach to the Labusch point $\kappa \to 1$, a more regular potential is required near the force maximum. The results of such an analysis for a cubic pin (or quadratic-force model), although analytically accessible in the static limit, are somewhat cumbersome and we refer the interested reader to Ref. [39].

Parabolic pin, linear-force model

A simple model for a strong pin is provided by the parabolic potential with the linear pinning-force restricted to a finite interval $[-\sigma,\sigma]$ [see Fig. 10(a)]

$$f_p(u) = \begin{cases} -f_p\, u/\sigma, & |u| < \sigma, \\ 0, & \text{otherwise.} \end{cases} \tag{97}$$

Given the jumps in the force at the boundaries $\pm\sigma$, the Labusch parameter $\kappa = f_p'(\pm\sigma)/\bar{C} \to \infty$ and the pin is strong for all values of f_p. As a consequence, any parabolic potential will produce vortex pinning, e.g., in numerical simulations [28]. On the other hand, the properties of the pin are determined by the dimensionless parameter [see Eq. (29) and the different sign used here]

$$\bar{\kappa} = -\partial_x f_p(x)/\bar{C} = f_p/\sigma\bar{C}, \tag{98}$$

which is of the same scale as the Labusch parameter κ for a similar smooth pin, but should not be confused with the Labusch parameter itself. Piecewise linear models of this type have been considered before in Ref. [13] using a simplified description of the system's elastic properties. Furthermore, Larkin and Ovchinnikov [14] used a periodic version of this model in a small-velocity analysis of the strong-pinning physics for large defects.

In the static situation, we have to solve the self-consistency equation (23) for the displacement field $u_s(x)$ and we obtain the result

$$u_s^f(x) = x, \quad |x| > x_s^f = \sigma, \tag{99}$$

$$u_s^p(x) = \frac{x}{1+\bar{\kappa}}, \quad |x| < x_s^p = \sigma(1+\bar{\kappa}), \tag{100}$$

with the jump points $-x_s^f$ and x_s^p for a right moving vortex separated by $\sigma(2+\bar{\kappa})$. The displacement field $u_s(x)$ then suddenly changes slope to generate the effective static force $f_p[u_s(x)] = -\bar{C}x/(1+\bar{\kappa}^{-1})$. Note that the jumps at $-x_s^f$ [by $\sigma\bar{\kappa}/(1+\bar{\kappa})$] and at x_s^p (by $\sigma\bar{\kappa}$) do not disappear for any values of $\bar{\kappa}$ and hence the pin is always strong. The critical force Eq. (24) assumes the value

$$\begin{aligned} F_c &= n_p f_p \frac{2t_\perp}{a_0^2} \int_{-x_s^f}^{x_s^p} \frac{dx}{\sigma} \frac{x}{1+\bar{\kappa}} \\ &= \frac{2\bar{\kappa}\sigma^2}{a_0^2} n_p f_p \frac{1+\bar{\kappa}/2}{1+\bar{\kappa}}, \end{aligned} \tag{101}$$

where we have used $t_\perp = x_s^f = \sigma$ in the last equation. The factor $2\bar{\kappa}\sigma^2$ should be interpreted as the trapping area $S_{\rm trap}$, see also Refs. [15,17].

Next, we turn to the low-velocity dynamics (see Fig. 10) and determine the coordinate shift $\delta x[u_s](x)$ inside the pinning interval $[-x_s^f, x_s^p]$, see Eq. (77),

$$\delta x[u_s](x) = -\frac{2}{\pi} \frac{\sigma\bar{\kappa}}{1+\bar{\kappa}} \frac{1+2x/\sigma}{\sqrt{1+x/\sigma}} \sqrt{\frac{v}{v_\sigma}}. \tag{102}$$

The divergence at $x = -\sigma$ is cut (at $\sim v t_{\rm th}$) by the fast single-vortex response at short times $t \sim t_{\rm th}$ where the 3D Green's function has to be replaced by the 1D one; the remaining spike is relevant in transforming the static solution $u_s(x)$ to the dynamic one $u(x)$. As compared with the result Eq. (77) above,

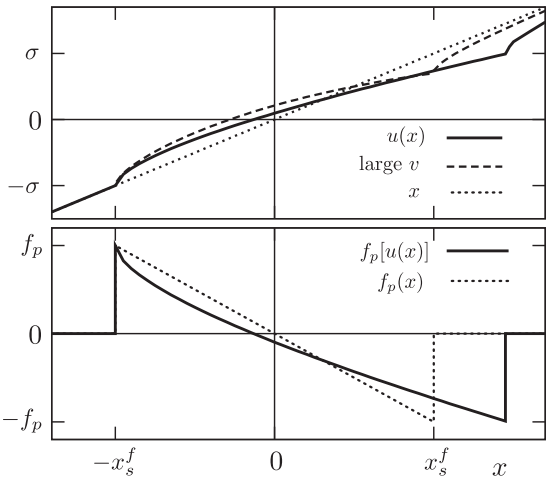

FIG. 11. Displacement field $u(x)$ and corresponding force $f_p[u(x)]$ at a high velocity $v/v_p = 2$ and for a pinning parameter $\bar{\kappa} = 2$. The exact results (solid lines) are compared with the high-velocity perturbative (dashed) and free (light dotted) results.

the coordinate shift for the linear force model does not exhibit any logarithmic corrections and hence there will be no term $\propto \sqrt{v}\ln v$ in the pinning-force density $\langle \delta F_p(v)\rangle$. In fact, using the result Eq. (102) in the calculation of the pinning-force density Eq. (73), we obtain

$$\langle \delta F_p(v)\rangle \approx -n_p f_p \frac{2t_\perp}{a_0^2}\left\{\int_{-x_s^f}^{x_s^p} \frac{dx}{\sigma}\,\frac{\delta x[u_s](x)}{1+\bar{\kappa}} - \delta x[u_s]\big(x_s^p\big)\right\}$$
$$= -\frac{4}{3\pi}\frac{\bar{\kappa}\sigma t_\perp}{a_0^2} n_p f_p \frac{5+5\bar{\kappa}+2\bar{\kappa}^2}{(1+\bar{\kappa})^2}\sqrt{\frac{v}{v_p}}, \qquad (103)$$

with $v_p = v_\sigma(2+\bar{\kappa})$ deriving from the effective pin size $\sigma(2+\bar{\kappa})$. As discussed above, the pinning force is reduced $\propto\sqrt{v/v_p}$ with respect to the static critical force in the strong pinning situation discussed here. A result similar to Eq. (103) was obtained by Larkin and Ovchinnikov [14] in a periodic linear model for large defects.

Going to the limit of high velocities $v \gg \bar{\kappa} v_p$, we first determine the lowest-order correction to the displacement field, see Eq. (54),

$$u_p(x) = -\frac{2\bar{\kappa}}{\pi}\frac{\partial}{\partial x}\int_{-\sigma}^{x} dx' x'\sqrt{\frac{x-x'}{vt_{\rm th}}}$$
$$= -\frac{2\bar{\kappa}\sigma}{3\pi}\sqrt{\frac{v_\sigma}{v}}\left(\frac{2x}{\sigma}-1\right)\sqrt{1+\frac{x}{\sigma}} \qquad (104)$$

for $-\sigma < x < \sigma$, see Fig. 11. Using the perturbative expression Eq. (47) for the pinning force [note that $f_p'(x)$ includes a δ function], we arrive at the result [cf. Eq. (55)]

$$\langle F_p(v)\rangle \approx \frac{12\sqrt{2}}{5\pi}\frac{\sigma t_\perp}{a_0^2} n_p f_p \sqrt{\frac{\bar{\kappa}^2 v_\sigma}{v}}. \qquad (105)$$

The linear-force model also allows for an *exact* solution of the dynamical situation; within the interval $u \in [-\sigma,\sigma]$ the

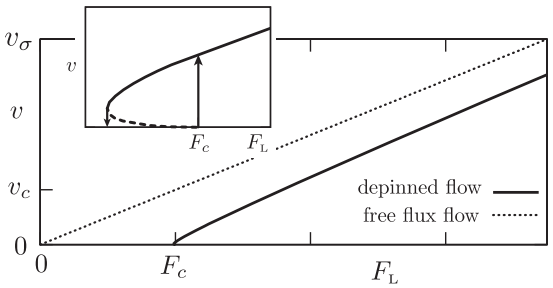

FIG. 12. The exact force-density-velocity (current-voltage) relation for parabolic pins with strength $\bar{\kappa} = f_p/\sigma\bar{C} = 2$. The pinning velocity scale $v_p = 2v_\sigma$ is much larger than the viscous velocity scale $v_c = F_c/\eta$. Note the bistability for values of the Lorentz force density $F_{\rm L}$ close to the critical force density F_c (inset), leading to the appearance of jumps [14]. This bistable regime extends over a region of size $\propto n_p^2$ both in force and in velocity. For large values of $F_{\rm L}$, free flux flow (dashed) is approached.

self-consistency equations (23) and (65) assume the form

$$u(x) = \frac{x-\delta x[u](x)}{1+\bar{\kappa}}, \qquad (106)$$

$$\delta x[u](x) = -\frac{f_p}{\sigma}\frac{\partial}{\partial x}\int_{-\sigma}^{x} dx' G^{\uparrow}(x-x')u(x'). \qquad (107)$$

This problem can be solved exactly via a Laplace transform and we obtain the solution [40]

$$u(z) = \frac{1}{z^2(1+\bar{\kappa}g(z))}, \qquad (108)$$

$$g(z) = e^{zvt_{\rm th}}\mathrm{erfc}(\sqrt{zvt_{\rm th}}), \qquad (109)$$

with $\mathrm{erfc}(x)$ the complementary error function. Unfortunately, the final solution involves an inverse Laplace transform which cannot be done in closed form,

$$u(x) = \frac{x-\bar{\kappa}\sigma}{1+\bar{\kappa}} + \sigma\bar{\kappa}\int_0^\infty \frac{ds}{\pi}\left(\frac{v/v_{\rm th}}{s^2}+\frac{1}{s}\right)$$
$$\times \frac{(1-e^{-s(1+x/\sigma)v_\sigma/v})e^{-s}\mathrm{erfi}(\sqrt{s})}{(1+\bar{\kappa}e^{-s})^2+\bar{\kappa}^2e^{-2s}\mathrm{erfi}^2(\sqrt{s})}, \qquad (110)$$

where $\mathrm{erfi}(x)$ denotes the imaginary error function. The result of the numerical evaluation of (110) is shown in Fig. 10, together with the results of the fast- and the slow-velocity analysis.

In the final step, we make use of the mean pinning-force density $\langle F_p(v)\rangle$ in the solution of the force-balance equation (1) and find the force-velocity characteristic, see Fig. 12. For small velocities $v \ll v_p$, the force balance equation assumes the form

$$\eta v + F_c(1-\beta\sqrt{v/v_p}) = F_{\rm L}, \qquad (111)$$

with

$$\beta = \frac{4}{3\pi}\frac{5+5\bar{\kappa}+2\bar{\kappa}^2}{(2+\bar{\kappa})(1+\bar{\kappa})} \xrightarrow{\bar{\kappa}\to\infty} \frac{8}{3\pi} \qquad (112)$$

determined from Eq. (103). The pinning-force density, decreasing with velocity via a square-root law, outperforms the linear behavior of the viscous force density ηv at small v. As

a consequence, the force-velocity relation is bistable with (we define the small parameter $\nu = \beta^2 v_c/4v_p \sim n_p \bar{\kappa}\sigma^2 a_0 \ll 1$)

$$\frac{v}{v_c} \approx \nu\left(1 \pm \sqrt{1 + \frac{1}{\nu}\frac{F_L - F_c}{F_c}}\right)^2. \tag{113}$$

Equation (113) describes an unstable characteristic $v/v_c \approx (1/4\nu)(1 - F_L/F_c)^2$ at small v and a jump $\delta v/v_c \approx 4\nu$ at $F_L = F_c$, see Fig. 12, as also noted by Larkin and Ovchinnikov in their pinning analysis of large defects [14]. The bistability regime extends over a region of size $\propto n_p^2$ both along the force- and along the velocity axes; specifically, bistability appears within the force interval $1 - \nu < F_L/F_c < 1$ and for velocities $v/v_c < 4\nu$. The electric field E_c corresponding to the jump velocity $4\nu v_c$ can be expressed through the critical current density j_c and the flux-flow resisitivity ρ_{ff}, $E_c = 4\nu\rho_{ff} j_c \sim (\kappa n_p \sigma^2 a_0)\rho_{ff} j_c$, with $\kappa n_p \sigma^2 a_0 \ll 1$ assuring the dilute pinning limit.

Above the critical drive $F_L - F_c \ll F_c$, we find the linear shape $v/v_c \approx F_L/F_c - 1$. Hence, the force-velocity relation is dominated by the static pinning-force density $F_c \propto n_p$ and the viscous force density ηv. For large velocities, we use $\langle F_p(v)\rangle$ from the expansion Eq. (105) and find the correction around flux flow

$$v \sim \frac{F_L}{\eta} - \frac{4\sqrt{2}}{3\pi}\frac{\bar{\kappa}\sigma t_\perp}{a_0^2}\frac{n_p f_p}{\eta}\sqrt{\frac{v_\sigma}{v_c}\frac{F_c}{F_L}}. \tag{114}$$

The linear-force model always resides in the strong pinning limit with $\kappa = \infty$. The most relevant point in the pinning process, the point $x_s^p = \sigma(\bar{\kappa} + 1)$ where the vortex jumps out of the pin, then coincides with the point of maximal (negative) force with $u_s(x_s^p) = \sigma$ at the pin boundary. In order to analytically study the dynamical pinning force at smaller values of κ including the approach to the Labusch point, one has to choose a smooth shape for the pinning potential. Demanding that the static limit is still analytically solvable, one may choose a cubic potential with the quadratic force profile

$$f_p(x) = f_p \begin{cases} -(x/\sigma)^2 - x/\sigma, & -\sigma < x < 0, \\ (x/\sigma)^2 - x/\sigma, & 0 < x < \sigma, \end{cases} \tag{115}$$

and zero otherwise. This model pin then comes with a tunable Labusch parameter

$$\kappa = \max_x \frac{\partial_x f_p(x)}{\bar{C}} = \frac{\partial_x f_p(\pm\sigma)}{\bar{C}} = \frac{f_p}{\sigma\bar{C}} \tag{116}$$

and can still be solved analytically in the static limit, that provides the basis for an approximate solution of its dynamical behavior. Since the results are rather cumbersome, we refer the reader to the original solution in Ref. [39].

VII. CONCLUSION

We have analyzed the dynamics of the vortex lattice in the presence of dilute strong pins characterized by a Labusch parameter $\kappa > 1$ and have determined the strong-pinning force-velocity (or current-voltage) characteristic in the single-pin single-vortex limit. The basic task is the solution of a nonlinear integral equation for the displacement field $u(x = vt)$ describing the vortex tip position when traversing the pin, while the vortex ends at $z \sim \pm\infty$ move with constant velocity v. The average $\langle f_p(v)\rangle$ over the individual pinning forces $f_p[u(x)]$ and a proper determination of the velocity dependence of the transverse trapping length $t_\perp(v)$ provide the velocity-dependent mean pinning-force density $\langle F_p(v)\rangle$. In a last step, we find the mean velocity $v(F_L)$ as a function of the driving Lorentz-force density F_L–the force-velocity or current-voltage characteristic–by solving the force balance equation $\eta v = F_L - \langle F_p(v)\rangle$.

The self-consistent dynamical integral equation for the displacement field $u(x)$ can be solved numerically by simple forward integration due to causality. Such a numerical solution has been carried out for the Lorentzian-shaped pinning potential in order to determine the dynamical effective pinning force $f_p[u(x)]$ and the dependence of the pinning force $\langle f_p(v)\rangle$ on the velocity v. In the static limit, the integral can be separated and the problem simplifies to an algebraic one. The appearance of a multi-valued static solution characterizes a strong pin and allows for a finite static critical force $f_c = \langle f_p(v = 0)\rangle$; the latter is a consequence of the asymmetric occupation of free and pinned branches as the moving vortex jumps into and out of the pin. At finite velocities, the jumps in the static solution $u_s(x)$ give way to a unique smooth and asymmetric solution $u(x)$ and the force $f_p[u(x)]$ derives from a direct integration without invoking an asymmetric occupation.

The velocity dependence of the dynamical pinning force $\langle f_p(v)\rangle$ is governed by the elastic properties of the vortex system as expressed through the Green's function. Its velocity scale is given by $v_p = \kappa v_\sigma = \kappa\sigma/t_{th}$, where κ and σ encode properties of the pins and t_{th} is the timescale for the dissipative relaxation of an elastic deformation. At small velocities, a perturbative treatment away from the static solution provides a decrease $\langle \delta f_p(v)\rangle \propto -\sqrt{v/v_p}$ of the mean pinning force at large values of $\kappa \gg 1$ and an increase $\langle \delta f_p(v)\rangle \propto \sqrt{v/v_p}$ for small values $\kappa \gtrsim 1$. Indeed, a correction of positive sign $\langle \delta f_p(v)\rangle \propto \sqrt{v/v_p}\log(v_p/v)$ shows up in a small region as $v \to 0$ for any value of κ, however, this region is exponentially small at large κ. Increasing the velocity beyond $(a_0/\lambda)^2 v_p$, the 3D bulk response gives way to a region of 4D dispersive behavior and $\langle \delta f_p(v)\rangle \propto v/v_p$ changes linearly with velocity. At high velocities $v > v_p$, the rapid motion is dominated by the 1D single-vortex response; furthermore, a self-consistent analysis of the problem shows that the longitudinal trapping or pinning length decreases from $\sim \kappa\sigma$ to $\sim \sigma$, producing a rapid drop in the pinning force $\langle f_p(v)\rangle \propto v_p/v$. The v_p/v decay of $\langle f_p(v)\rangle$ extends over a large velocity regime $v_p < v < \kappa v_p$ and has not been known before. Finally, perturbation theory away from free flux flow can be performed at high velocities $v \gg \kappa v_p$ where pinning is always effectively weak and which provides a force decaying as $\langle f_p(v)\rangle \propto (\kappa v_p/v)^{1/2}$.

The pinning-force density $\langle F_p(v)\rangle \approx n_p(2t_\perp(v)/a_0)\langle f_p(v)\rangle$ follows from simple averaging via direct summation over independent pins, once the dynamical transverse pinning length $t_\perp(v)$ has been determined. The latter can be found by studying the trapping process for a vortex approaching the defect with a finite impact parameter and at finite velocity; it turns out that the trapping length decreases from its static value $t_\perp \sim \sigma\kappa^{1/(n+2)}$ to $t_\perp \sim \sigma$ as the velocity increases to v_p.

Our study provides access to several types of results: (i) exact ones deriving from numerical integration for specific defect potentials $e_p(r)$ and (ii) perturbative analytic results in the static- and high-velocity limits. Quite remarkable are (iii) the universal results obtained in the large-κ limit, with a linear force $f_p[u_s(x)] \approx -\bar{C}x$ appearing in the static limit and a square-root force $f_p[u(x)] \approx -(2/\pi)\bar{C}\sqrt{vt_{\rm th}x}$ in the intermediate velocity regime $v_p < v < \kappa v_p$. Finally, (iv) dimensional estimates provide us with simple qualitative results for the evolution of $\langle F_p(v)\rangle$ with changing velocity v and for all values of κ. (v) Numerical and analytic calculations for a parabolic model-potential give additional insights into the pinning dynamics. Such parabolic pins have often been used in numerical simulations of vortex dynamics in disorder landscapes [28] and always reside in the strong-pinning limit due to their sharp boundary.

The analysis of the velocity-dependent pinning-force density $\langle F_p(v)\rangle$ provides us with the velocity scale v_p governing the relaxation of the vortex motion across the pinning centers. In the limit of a dilute density n_p of pins (where pinning centers act individually) this velocity is much larger than the velocity scale $v_c = F_c/\eta$ describing the overall motion of the vortex system after depinning. It is this separation of velocities that produces a simple force-velocity or current-voltage characteristic in the strong pinning situation with a dilute density of pins: after depinning at F_c (or j_c), the characteristic evolves first in parallel to free flux flow [excess-force characteristic $v \sim (F_{\rm L} - F_c)/\eta$] and approaches the free flow behavior $v \sim F_{\rm L}/\eta$ only at very high velocities $v > v_p \gg v_c$. With our derivation of the excess-force characteristic for the strongly-pinned vortex system in the dilute-pin limit, we have derived the analogue of Coulomb's law of dry friction for strong vortex pinning—it would be interesting to see if the ideas leading to this result could be applied to other problems of dry friction. Additional nonlinear corrections (corresponding to corrections of Coulomb's law), a jump at very strong pinning with $\kappa \gg 1$ and a smooth onset for $\kappa \gtrsim 1$ appear in a narrow region of size $\propto n_p^2$ near depinning; however, a word of caution is in place as results in this regime may get modified by collective pinning effects.

Our theoretical results compare well to a number of experimentally measured current-voltage characteristics [23–27]. The linear excess-current characteristic reported in early experiments was discussed by Campbell and Evetts [7] and by Campbell [12], however, no microscopic derivation of this basic result has been provided so far. In these experiments, the excess current-voltage characteristic could be observed over a large drive interval without suffering from thermal breakdown effects. Indeed, observing this type of characteristic requires to push the current up to roughly twice its critical value in order to reach a velocity of order v_c. In order to avoid heating, samples with low values of j_c, consistent with our small n_p condition, are beneficial, see e.g., Ref. [25].

Unfortunately, one has to admit that even today, no systematic studies of experimental current-voltage characteristics are available: given a specific material, the defect structure is usually nontrivial and may include a variety of pin types. Furthermore, the parameters characterizing the defects are difficult to find. Experiments with superconductors where defects could be designed, tuned, and properly characterized would provide a great help and motivation in further developing the theory of pinning and allow a better comparison between theory and experiment. Numerical studies based on the time-dependent Ginzburg-Landau theory and aiming at optimizing the pinning landscape have been performed very recently [36] and it will be interesting to compare our results with this type of numerical effort.

Further work is required on the theoretical side. With our analysis, we have provided an important step in the understanding of the static and dynamical strong pinning behavior and its crossover to weak pinning. However, our study is limited to the single-pin single-vortex situation and one has to include effects of other vortices and correlations between pins in order to arrive at a complete picture. Correlations between pins will generate higher-order corrections in n_p both in the static and the low-velocity dynamic behavior and their inclusion is a crucial element in the full understanding of the weak to strong pinning crossover.

ACKNOWLEDGMENTS

We gratefully acknowledge the foundational contribution of the late Anatoli Larkin to this field of study. We thank Roland Willa and Martin Buchacek for numerous discussions and financial support of the Swiss National Science Foundation through the Division II and the National Centre of Competence in Research 'MaNEP—Materials with Novel Electronic Properties.'

APPENDIX A: CORRECTIONS TO THE UNIVERSAL STATIC SOLUTION

In this appendix, we improve the accuracy of the universal static solution in Sec. III C and further investigate the behavior of the vortex near depinning. In order to find the static force profile $f_p[u_s(x)]$ near depinning at x_s^p, we make use of Eq. (23) and expand the bare potential $f_p(x)$ in the relevant region around its minimum (near the maximal pinning force pointing along $-x$). We characterize the minimum in the bare pinning force $f_p(x)$ (i.e., its largest negative value) through its position σ_m, the maximum (negative) pinning force $-f_p$, and the (positive) curvature $f_p'' = f_p/\sigma^2$,

$$f_p(x) \approx -f_p + \frac{f_p}{2\sigma^2}(x-\sigma_m)^2. \tag{A1}$$

Note that, here, the parameter $\sigma \equiv (f_p''(\sigma_m)/f_p)^{1/2}$ is a precisely defined model parameter that agrees with the previous (loose) definition as the pin size for the situation where the defect potential involves only one length scale. In order to relate the static displacement field u_s to the asymptotic coordinate x, we combine the above ansatz for the bare pinning force $f_p(x)$ with the static self-consistency equation (23). Replacing $x \to u_s$ in Eq. (A1) and using (23), $\bar{C}(u_s - x) = f(u_s)$, we find the static displacement field

$$u_s(x) \approx \sigma_m + \frac{\sigma}{\bar{\kappa}} - \sqrt{\frac{2\sigma}{\bar{\kappa}}\left(x_s^p - x\right)} \tag{A2}$$

with $\bar{\kappa} \equiv f_p/\sigma\bar{C}$ and $x_s^p \equiv \bar{\kappa}\sigma + \sigma_m + \sigma/2\bar{\kappa} \approx \bar{\kappa}\sigma$ the depinning point, see Fig. 5. Making use of Eq. (23) once more, we

obtain the static pinning force

$$f_p[u_s(x)] \approx -\bar{C}x + f_p \frac{u_s(x)}{\bar{\kappa}\sigma}, \tag{A3}$$

with the last term a correction of order $\sim f_p/\bar{\kappa}$. This force profile decreases linearly with slope $\bar{C}$ up to $x \approx \bar{\kappa}\sigma$, reaches its minimum $-f_p$ (the maximum backward force f_p) at $x = \bar{\kappa}\sigma + \sigma_m$ and increases by $f_p/2\bar{\kappa}^2$ when x increases further by $\sigma/2\bar{\kappa}$ in order to diverge upwards at $x = x_s^p$, see Fig. 5.

In summary, at very strong pinning (by a defect with tails), we find a universal static solution where the vortex jumps into the pin at $-x_s^f \sim -\kappa^{1/(n+2)}\sigma$ and then is deformed linearly in x, with the vortex tip remaining trapped in the pin. The elastic energy of this deformation balances the effective pinning force $-\bar{C}x$. The backward pointing tip remains fixed onto the defect until reaching the largest force $-f_p$ with the vortex stretched by $\sim \kappa\sigma$, see Fig. 5. When the force decreases again in magnitude, the vortex remains attached to the pin over the short distance $\sim \sigma/2\kappa$ and then depins with a sharp forward jump in $u_s(x)$ at x_s^p, from $u_s \sim \sigma$ before to $u_s \sim \kappa\sigma$ after depinning. With this jump, the vortex tip depins and ends on the free branch where it experiences a small residual force $f_p(x_s^p) \sim -f_p/\kappa^{n+1} < 0$. For a vortex with a finite impact parameter and a radially symmetric defect potential, the above scenario is still valid, with the vortex jumping into and out of the pin at the radii $R_s^f = x_s^f$ and $R_s^p = x_s^p$. Note that at very strong pinning, jumping into and out of the pin are very asymmetric processes, with the vortex jumping into the pin anywhere along the semicircle with radius R_s^f, while it jumps out of the pin in a narrow, forward directed angle, see Fig. 2. Hence the depinning process [that determines $\langle f_p(v)\rangle$] does not depend much on the impact parameter b.

APPENDIX B: WEAK COLLECTIVE VERSUS SINGLE PINS

Here, we comment on the relation between weak collective pinning theory and our single-pin approximation pertinent to the strong pinning paradigm. The perturbative result (48) for the average pinning-force density $\langle F_p(v)\rangle$ obtained within our single-pin (SP) analysis coincides, to lowest order in κ and in the pin density n_p, with the result obtained from weak collective pinning theory [10] (WCP). On a first glance, this result may appear as a surprise, however, the correlations manifest in Eq. (48) arise quite naturally when constructing a pinning landscape with a finite density n_p of randomly distributed pins with a pinning potential $\varepsilon_p(\mathbf{r})$, see Eq. (4). The pinning energy density $E_p[\mathbf{r},\mathbf{u}]$ of such a disorder landscape can be written as

$$\begin{aligned} E_p[\mathbf{r},\mathbf{u}] &= \sum_{\mu,i} e_p(\mathbf{R}_\mu + \mathbf{u}_\mu(z) - \mathbf{R})\, \delta^3(\mathbf{r} - \mathbf{r}_i) \\ &= \sum_{\mu} e_p(\mathbf{R}_\mu + \mathbf{u}_\mu(z) - \mathbf{R})\, \rho_p(\mathbf{r}) \end{aligned} \tag{B1}$$

with the pin density

$$\rho_p(\mathbf{r}) = \sum_i \delta^3(\mathbf{r} - \mathbf{r}_i). \tag{B2}$$

The corresponding force field $\mathbf{F}_p[\mathbf{r},\mathbf{u}]$ relates to Eq. (5) via

$$\int \frac{d^2R}{a_0^2} \mathbf{F}_p[\mathbf{r},\mathbf{u}] = \sum_\mu \mathbf{F}_p(\mathbf{r}_\mu,\mathbf{u}_\mu). \tag{B3}$$

Assuming *self-averaging*, the average pinning-force density $\langle \mathbf{F_p}\rangle$ in Eq. (5) then can be written as the volume average

$$\langle \mathbf{F_p}\rangle = -\frac{1}{V}\int d^3r\, \mathbf{F}_p[\mathbf{r},\mathbf{u}]. \tag{B4}$$

Rewriting $\mathbf{u} = \mathbf{v}t + \mathbf{u}_p$ and expanding in $\mathbf{u}_p$ one obtains (for a drive along x)

$$\begin{aligned} \langle F_{p,x}\rangle = -\frac{1}{V}\int d^3r \int d^3r' \int^t dt'\, \partial_\alpha \partial_x E_p(\mathbf{r},\mathbf{v}t) \\ \times G_{\alpha\beta}(\mathbf{r}-\mathbf{r}', t-t')\, \partial_\beta E_p(\mathbf{r}',\mathbf{v}t'). \end{aligned} \tag{B5}$$

Inserting the form (B1) of the pinning energy landscape and assuming small and weak pinning defects, the sums over pairs of vortices ν and μ and pairs of pins i and j reduce to those terms with $\mu = \nu$ and $i = j$; expressing the sums over vortices and pinning centers as integrals over d^2R/a_0^2 and $n_p d^3r_p$, we arrive at

$$\begin{aligned} \langle F_{p,x}\rangle = -n_p \int^t dt'\, G(0,t-t') \\ \times \int \frac{d^2R}{a_0^2}\, \partial_\alpha \partial_x e_p[\mathbf{R}+\mathbf{v}t]\, \partial_\alpha e_p[\mathbf{R}+\mathbf{v}t'], \end{aligned} \tag{B6}$$

which, choosing the time $t = 0$, is easily reduced to the result Eq. (48). Alternatively, one may take the average over disorder realizations on the right hand side of Eq. (B5), represent the pinning energy density E_p through Eq. (B1), and use the density-density correlator

$$\langle \rho(\mathbf{r})\rho(\mathbf{r}')\rangle = n_p^2 + n_p \delta^3(\mathbf{r}-\mathbf{r}'). \tag{B7}$$

The pinning energy correlator then is easily reduced to the usual form (the reducible term n_p^2 in Eq. (B7) is irrelevant in the present discussion)

$$\langle E_p(\mathbf{r},\mathbf{u}) E_p(\mathbf{r}',\mathbf{u}')\rangle = \delta^3(\mathbf{r}-\mathbf{r}') K(\mathbf{u}-\mathbf{u}') \tag{B8}$$

with the $K(\mathbf{u})$ given by Eq. (49) (again, we use that individual pins are small and weak, such that the sum over vortex pairs reduces to a single sum over $\mu = \nu$). Hence the single-pin result (48) contains all the correlations present in the disorder landscape described by Eq. (B1).

The single-pin approach predicts a vanishing critical force F_c for $\kappa < 1$, while the weak collective pinning scheme provides a finite result. This difference arises due to the different handling of the small velocity limit in the two approaches. In the weak pinning scenario, we stop decreasing the velocity v when perturbation theory breaks down as the pinning-induced correction δv becomes of order of the velocity v itself; the criterion $\delta v \sim v \equiv v_c$ defines a finite (critical) pinning-force density $F_c^{\rm WCP} \equiv \langle F_p(v_c)\rangle$. In the strong pinning scenario, instead, we take v all the way to zero and obtain a vanishing critical force density $F_c^{\rm SP} = 0$. On the other hand, using the SP result, Eq. (47), and adopting the WCP cutoff scheme, we find a finite critical current density j_c as well: with the estimate $\langle F_p(v)\rangle^{\rm SP} \sim n_p(\sigma/\lambda)(f_p^2/\varepsilon_0)(v/v_\sigma)^{1/2}$ from Eq. (53), valid at low velocities, and the conditions $\langle F_p(v_c)\rangle^{\rm SP} \sim \eta v_c \sim j_c B/c$, we obtain the critical current density (with $j_0 \sim c\varepsilon_0/\Phi_0\xi$

denoting the depairing current density and using $\sigma \sim \xi$)

$$j_c \sim j_0(\xi^2/\lambda^2)\left(n_p a_0^3 f_p^2/\varepsilon_0^2\right)^2 \propto n_p^2, \tag{B9}$$

in agreement with the results obtained from weak collective pinning theory [17]. This result is quite remarkable: first, the critical current (B9) is proportional to n_p^2, the *square* of the pin density n_p, i.e., its origin is in the correlations between pins. Second, the result is still consistent with the standard SP result $\langle F_p(v=0)\rangle^{\rm SP} = 0$, as the latter is an order n_p result and corrections $\propto n_p^2$ are beyond the standard SP approach. For strong pinning $\kappa > 1$, we already obtain a finite critical force $\langle F_p(v=0)\rangle^{\rm SP} \propto n_p$, *linear* in pin density. In this situation, pin-pin correlations are expected to provide corrections $o(n_p)$, which vanish faster than linear, allowing us to approach the critical force parametrically closer than in the WCP situation.

APPENDIX C: AVERAGE PINNING FORCE AT SMALL VELOCITIES

In this appendix, we bring the expression (71) for the average pinning force to a manageable form. Out of the five terms in Eq. (71), we can drop the first and last integrals. For a compact pin, the force is small, of order f_p/κ just before $-x_s^f$ and negligible on the free branch at x_s^p, see the discussion in Sec. III C above. The first integral then is small by the factor $\kappa^{-3/2}$ as compared to the main terms, while the last integral is exponentially small. For a Lorentzian pin with large tails, the force is of order $f_p/\kappa^{3/4}$ at $-x_s^f$; it contributes a term smaller by $\kappa^{-9/8}$ as compared to the leading terms. In the last integral, the force starts at a value of order $-f_p/\kappa^3$ and its contribution is small by the factor κ^{-6}.

The second term describes the part of the jump into the pin when the dynamic solution has not yet responded to the presence of the pin, while the static solution has already jumped. This term scales the same way as the first integral; for a compact pin of size σ, the pinning force f_p/κ is still small and the term is small by a factor $\kappa^{-3/2}$, while for a Lorentzian pin its contribution is small by the factor $\kappa^{-9/8}$ and can be safely ignored as well.

The important terms are the third and fourth ones describing the change in the pinning force as the vortex moves through the pin and the force difference arising from the substantial change in the location of depinning, respectively,

$$\langle \delta f_p(v)\rangle \approx -\frac{1}{a_0}\left[\int_{-x^f}^{x^p} dx\, \delta f_{pp}(x) + \int_{x^p}^{x_s^p} dx\, \delta f_{fp}(x)\right]. \tag{C1}$$

In order to analyze this expression further, we have to investigate the behavior of the coordinate shift $\delta x[u](x)$, see Eq. (65). This shift is small, $\propto \sqrt{v}$, over most of the pinning interval $[-x^f, x^p]$, where the (small) velocity parameter arises from the integrated Green's function $G^\uparrow(x = vt)$, see the third line of Eq. (67). A notable exception are the two spikes at $-x^f$ and at x^p where the vortex jumps into and out of the pin. These spikes are large, of size $x_s^p - x_s^f \sim \sigma\kappa$, but extend only over a small interval $\sim v t_{\rm th}$, see (61).

Away from these spikes, we can approximate the coordinate shift $\delta x[u](x)$ by $\delta x[u_s](x)$. In fact, the difference $\delta x[u](x) - \delta x[u_s](x)$ involves the force difference $f_p[u(x)] - f_p[u_s(x)]$ as it appears in the correction $\langle \delta f_p(v)\rangle$ given by Eq. (70) above, multiplied with the Green's function $G^\uparrow(x) \propto \sqrt{v/v_\sigma}$, see Eq. (67). Taking the coordinate x through the various regimes, one can show that $\delta x[u](x) \approx \delta x[u_s](x)$ to order v away from the jumps (with one factor $\sqrt{v}$ originating from the force difference and another from the Green's function $G^\uparrow$) and to order $\sqrt{v}$ in a region of order $\sqrt{v}$ near the jumps (we ignore the region of size $v t_{\rm th}$ at the jumps where the difference is of order $\sigma\kappa$). Furthermore, we can replace (to precision $\sqrt{v}$) the positions $-x^f$ and x^p by their static counterparts,

$$x_s^f - x^f = \delta x[u](-x^f) \approx \delta x\left[u_s^f\right]\left(-x_s^f\right) \propto \sqrt{v}, \tag{C2}$$

and similarly (note that we have to make sure that we always stay on well-defined, continuous branches)

$$x_s^p - x^p = -\delta x[u](x^p) \approx -\delta x\left[u_s^p\right]\left(x_s^p\right) \propto \sqrt{v}. \tag{C3}$$

In simplifying Eq. (C1), we make use of the smallness of $\delta x[u](x)$ in the interval $[-x^f, x^p]$ and expand the integrand $\delta f_{pp}(x) \approx \partial_x f_p[u_s^p(x)]\,\delta x[u](x)$. Next, we replace (to lowest order in v) the unknown dynamical quantities $u(x)$, x^f, and x^p by the known static expressions $u_s(x)$, x_s^f, and x_s^p. Finally, we replace the second integral by the product of force difference $\delta f_{fp}(x) \approx f_p[u_s^f(x_s^p)] - f_p[u_s^p(x_s^p)]$ times the width $x_s^p - x^p \approx -\delta x[u_s^p](x_s^p)$ of the integration region, exploiting the sharp decay of both $f_p[u_s(x)]$ and $f_p[u(x)]$ at the boundaries. While the former is a property of the static solution, that latter is guaranteed by the smallness of the depinning length $x_{\rm dp} \propto v$, see Eq. (61). We then arrive at the closed expression (73) that we use in the main text to derive the $\propto\sqrt{v/v_p}$ corrections to the average pinning force.

[1] H. Kamerlingh Onnes, Proc. K. Ned. Akad. Wet. **13**, 1274 (1911); **14**, 820 (1912).

[2] W. Meissner and R. Ochsenfeld, Naturwissenschaften **21**, 787 (1933).

[3] L. V. Shubnikov, V. I. Khotkevich, Y. D. Shepelev, and Y. N. Riabinin, Zh. Eksp. Teor. Fiz. **7**, 221 (1937) [Ukr. J. Phys. **53**, 42 (2008)].

[4] A. A. Abrikosov, Zh. Eksp. Teor. Fiz. **32**, 1442 (1957) [Sov. Phys. JETP **5**, 1174 (1957)].

[5] J. Bardeen and M. J. Stephen, Phys. Rev. **140**, A1197 (1965).

[6] R. Labusch, Cryst. Lattice Defects **1**, 1 (1969).

[7] A. M. Campbell and J. E. Evetts, Adv. Phys. **21**, 199 (1972).

[8] A. I. Larkin and Yu. N. Ovchinnikov, J. Low Temp. Phys. **34**, 409 (1979).

[9] A. I. Larkin, Zh. Eksp. Teor. Fiz. **58**, 1466 (1970) [Sov. Phys. JETP **31**, 784 (1970)].

[10] G. Blatter, M. V. Feigel'man, V. B. Geshkenbein, A. I. Larkin, and V. M. Vinokur, Rev. Mod. Phys. **66**, 1125 (1994).

[11] E. H. Brandt, Rep. Prog. Phys. **58**, 1465 (1995); T. Nattermann and S. Scheidl, Adv. Phys. **49**, 607 (2000).

[12] A. M. Campbell, Philos. Mag. B **37**, 149 (1978).

[13] T. Matshushita, E. Kusayanagi, and K. Yamafuji, J. Phys. Soc. Jpn. **46**, 1101 (1979); T. Matshushita, *ibid.* **46**, 1109 (1979); T. Matshushita and K. Yamafuji, *ibid.* **47**, 1426 (1979); **50**, 38 (1981).

[14] A. I. Larkin and Yu. N. Ovchinnikov, in *Nonequilibrium Superconductivity*, edited by D. N. Langenberg and A. I. Larkin (Elsevier, Amsterdam, 1986), p. 493.

[15] Yu. N. Ovchinnikov and B. I. Ivlev, Phys. Rev. B **43**, 8024 (1991).

[16] A. E. Koshelev and A. B. Kolton, Phys. Rev. B **84**, 104528 (2011).

[17] G. Blatter, V. B. Geshkenbein, and J. A. G. Koopmann, Phys. Rev. Lett. **92**, 067009 (2004).

[18] R. Willa, V. B. Geshkenbein, R. Prozorov, and G. Blatter, Phys. Rev. Lett. **115**, 207001 (2015); R. Willa, V. B. Geshkenbein, and G. Blatter, Phys. Rev. B **92**, 134501 (2015).

[19] R. Willa, V. B. Geshkenbein, and G. Blatter, Phys. Rev. B **93**, 064515 (2016).

[20] A. Schmid and W. Hauger, J. Low Temp. Phys. **11**, 667 (1973).

[21] A. I. Larkin and Yu. N. Ovchinnikov, Zh. Eksp. Teor. Fiz. **65**, 1704 (1973) [Sov. Phys. JETP **38**, 854 (1974)].

[22] O. Narayan and D. S. Fisher, Phys. Rev. B **46**, 11520 (1992); P. Chauve, T. Giamarchi, and P. Le Doussal, *ibid.* **62**, 6241 (2000).

[23] A. R. Strnad, C. F. Hempstead, and Y. B. Kim, Phys. Rev. Lett. **13**, 794 (1964); Y. B. Kim, C. F. Hempstead, and A. R. Strnad, Phys. Rev. **139**, A1163 (1965).

[24] R. P. Huebener, *Magnetic Flux Structures in Superconductors* (Springer-Verlag, Berlin, 1979).

[25] P. Berghuis and P. H. Kes, Phys. Rev. B **47**, 262 (1993).

[26] Z. L. Xiao, E. Y. Andrei, Y. Paltiel, E. Zeldov, P. Shuk, and M. Greenblatt, Phys. Rev. B **65**, 094511 (2002).

[27] S. Pace, G. Filatrella, G. Grimaldi, and A. Nigro, Phys. Lett. A **329**, 379 (2004).

[28] C. Reichhardt, C. J. Olson, J. Groth, S. Field, and F. Nori, Phys. Rev. B **52**, 10441 (1995); C. J. Olson Reichhardt, Y. L. Wang, Z. L. Xiao, W. K. Kwok, D. Raya, C. Reichhardt, and B. Jankó, Physica C **533**, 148 (2017).

[29] A. U. Thomann, V. B. Geshkenbein, and G. Blatter, Phys. Rev. Lett. **108**, 217001 (2012).

[30] E. V. Thuneberg, J. Kurkijärvi, and D. Rainer, Phys. Rev. B **29**, 3913 (1984).

[31] A. Schmid, Phys. Kondens. Materie **5**, 302 (1966).

[32] J. R. Clem, J. Low Temp. Phys. **18**, 427 (1975).

[33] Note that we distinguish defect and vortex positions only by roman and greek indices, implying that these are not to be replaced by equal numbers.

[34] We point out a typo and a mistake in Ref. [19], where it should read $\int dz[\varepsilon_l(\partial_z u)^2/2 + V_{\rm cage}(u)]$ and $\bar{C} = 2\sqrt{2\pi\varepsilon_0\varepsilon_l}/a_0 = 2\sqrt{2\pi\ln(a_0/\xi)}\varepsilon_0/a_0$.

[35] A. Schönenberger, A. Larkin, E. Heeb, V. Geshkenbein, and G. Blatter, Phys. Rev. Lett. **77**, 4636 (1996).

[36] I. A. Sadovskyy, Y. Jia, M. Leroux, J. Kwon, H. Hu, L. Fang, C. Chaparro, S. Zhu, U. Welp, J.-M. Zuo, Y. Zhang, R. Nakasaki, V. Selvamanickam, G. W. Crabtree, A. E. Koshelev, A. Glatz, and W.-K. Kwok, Adv. Mater. **28**, 4593 (2016).

[37] C. M. Bender and S. A. Orszag, in *Advanced Mathematical Methods for Scientists and Engineers* (McGraw-Hill, New York, 1978), p. 150.

[38] Note that the limit $\kappa \to 1$ at fixed n_p would take us out of the single-pin regime: while $F_c^{\rm SP}(\kappa \to 1) \to 0$, $F_c^{\rm WCP}$ stays finite. The condition to remain in the strong pinning regime then reads $F_c^{\rm SP} > F_c^{\rm WCP}$, which requires that $(\kappa-1)^2/\kappa > (a_0/\lambda_0)^2(f_p/\varepsilon_0)^3(n_p a_0^4/\sigma)$.

[39] A. Thomann, Ph.D. thesis, ETH, 2011.

[40] We define the Laplace transform as $f(z) = \int_0^\infty dx \exp(-zx) f(x)$ and its inverse via $f(x) = \int_{\gamma-i\infty}^{\gamma+i\infty}(dz/2\pi i)\exp(zx) f(z)$.